

Louisiana Tech University

Louisiana Tech Digital Commons

Master's Theses


Graduate School

Winter 2020

Electrochemical Detection of Reactive Oxygen Species via a Platinum Microelectrode Array

Victor M. Carriere Jr.

Follow this and additional works at: <https://digitalcommons.latech.edu/theses>

 Part of the [Biomedical Engineering and Bioengineering Commons](#), and the [Electrical and Computer Engineering Commons](#)

**ELECTROCHEMICAL DETECTION OF REACTIVE
OXYGEN SPECIES VIA A PLATINUM
MICROELECTRODE ARRAY**

by

Victor M. Carriere, Jr., B.S.

A Thesis Presented in Partial Fulfillment
of the Requirements of the Degree
Master of Science

COLLEGE OF ENGINEERING AND SCIENCE
LOUISIANA TECH UNIVERSITY

March 2020

LOUISIANA TECH UNIVERSITY
THE GRADUATE SCHOOL

NOVEMBER 14, 2019

Date

We hereby recommend that the thesis prepared under our supervision by
Victor M. Carriere, Jr., B.S.

entitled Electrochemical Detection of Reactive Oxygen Species via a Platinum
Microelectrode Array

be accepted in partial fulfillment of the requirements for the Degree of
Master of Science in Biomedical Engineering

Supervisor of Thesis Research

Head of Department

Department

Recommendation concurred in:

Advisory Committee

Approved:

Approved:

Director of Graduate Studies

Dean of the Graduate School

Dean of the College

ABSTRACT

Oxidative stress, an excess of endogenous or exogenous reactive oxygen species (ROS) in the body, is closely aligned with inflammatory responses. ROS such as hydrogen peroxide, superoxide, and radical hydroxyl ion serve essential functions in fighting infection, but chronic elevation of these species irreversibly damages cellular components. Given the central role of inflammation in a variety of diseases, including Alzheimer's Disease, atherosclerosis, and rheumatoid arthritis, a low-cost, extracellular, non-invasive assay of ROS is needed.

This work reports the use of a platinum microelectrode array (Pt MEA)-based ceramic probe to detect time- and concentration-dependent variations in hydrogen peroxide (H_2O_2) production by activated macrophages. RAW 264.7 cells were placed under oxidative stress by activation with lipopolysaccharides (LPS). Chronoamperometry was then employed to detect the quantity of H_2O_2 released by cells at various time intervals up to 48 hours. The most stimulatory concentration of LPS was first identified. Further experiments assessed the anti-inflammatory effect of dexamethasone (Dex), a commonly prescribed steroid medication. As expected, the probe detected significantly increased H_2O_2 production by LPS-doped macrophages. This pro-inflammatory effect was diminished, but not resolved, in LPS-doped cells treated with Dex.

The long-term goal of this research is the development of a non-invasive, robust, multiplexed, point-of-care test of ROS and inflammation. Given the robustness of the

materials and the ease of modifying additional microelectrodes within the same probe, these results indicate that the probe is a suitable candidate for further study.

APPROVAL FOR SCHOLARLY DISSEMINATION

The author grants to the Prescott Memorial Library of Louisiana Tech University the right to reproduce, by appropriate methods, upon request, any or all portions of this Thesis. It is understood that “proper request” consists of the agreement, on the part of the requesting party, that said reproduction is for his personal use and that subsequent reproduction will not occur without written approval of the author of this Thesis. Further, any portions of the Thesis used in books, papers, and other works must be appropriately referenced to this Thesis.

Finally, the author of this Thesis reserves the right to publish freely, in the literature, at any time, any or all portions of this Thesis.

Author _____

Date _____

DEDICATION

This work is dedicated to my family, for whose love and patience I am always grateful.

TABLE OF CONTENTS

ABSTRACT.....	iii
APPROVAL FOR SCHOLARLY DISSEMINATION	v
DEDICATION	vi
LIST OF FIGURES	x
LIST OF TABLES	xiii
ACKNOWLEDGMENTS	xiv
CHAPTER 1 INTRODUCTION.....	1
1.1 Oxidative Stress	1
1.1.1 Introduction.....	1
1.1.2 Oxidative Stress and Inflammation.....	2
1.1.3 ROS and Reduction Potential	2
1.2 Overview of Major ROS/RNS.....	3
1.2.1 Superoxide ($\bullet\text{O}_2^-$)	3
1.2.2 Radical Hydroxyl Ion ($\bullet\text{OH}$).....	4
1.2.3 Nitric Oxide ($\bullet\text{NO}$).....	5
1.2.4 Hydrogen Peroxide	6
1.3 Role of Macrophages in Inflammation	7
1.3.1 Overview.....	7
1.3.2 The M1/M2 Paradigm of Macrophage Polarization.....	8
1.3.3 Professional Phagocytes and the Respiratory Burst.....	9
1.3.4 Selection of Cell Line for This Project	9

1.4	Chronoamperometry	10
1.4.1	Use of Chronoamperometry in Industrial Detection of H ₂ O ₂	11
1.4.2	Use of Chronoamperometry in Real-Time Detection of H ₂ O ₂ Release.....	11
1.5	Project Overview	12
1.5.1	Typical Methods of ROS Detection.....	12
1.5.1.1	Intracellular Methods.....	12
1.5.1.2	Extracellular Methods.....	13
1.5.2	Project Rationale.....	13
CHAPTER 2 METHODS		17
2.1	Fabrication and Preparation of Pt MEA Probes.....	17
2.1.1	Fabrication	17
2.1.2	Cleaning	18
2.1.3	Application of MPD Layer	18
2.2	Cell Culture.....	19
2.2.1	Maintenance of Cells in Culture	19
2.2.2	Plating of RAW 264.7 Cells	19
2.3	Treatment of Cells with Lipopolysaccharide (LPS) or Dexamethasone	20
2.3.1	Method 1	20
2.3.2	Method 2	21
2.4	Setup and Use of the Probe.....	21
2.4.1	Calibration in the Presence of H ₂ O ₂	21
2.4.2	Detection of Extracellular H ₂ O ₂	22
CHAPTER 3 RESULTS AND DISCUSSION.....		25
3.1	Calibration of the Probe in the Presence of H ₂ O ₂	25
3.2	Optimization of LPS Doping Protocol.....	27

3.2.1	Modification of Method 1	27
3.2.2	Proof of Concept – Method 2.....	29
3.2.3	Optimization of LPS Concentration.....	31
3.2.4	Optimization of Incubation Time.....	32
3.2.5	Optimization of Incubation Temperature.....	33
3.2.6	Effect of Dexamethasone on H ₂ O ₂ Production.....	34
3.2.7	Effect of Cell Culture Plate Type on H ₂ O ₂ Production.....	36
3.2.8	Viability Assay of LPS-Doped and ROS-Probed Cells.....	37
3.2.9	Optimization of the Calibration Protocol.....	39
CHAPTER 4 CONCLUSIONS AND FUTURE DIRECTIONS		40
APPENDIX A MATLAB SCRIPT FOR DATA ANALYSIS		41
BIBLIOGRAPHY		51

LIST OF FIGURES

- Figure 1-1:** Image from Kalyanaraman, B. [2]. Engulfing and oxidation of bacteria by an activated macrophage. In this example of respiratory burst, superoxide anions oxidize microbes directly, while also dismutating to O_2 and H_2O_2 . H_2O_2 also reacts with chloride anions to form hypochlorite ($HOCl$), a potent microbicidal oxidant..... 2
- Figure 1-2:** Redox cycling of two cysteine (Cys) residues within a redox-sensitive target protein (image from [22]). The H_2O_2 -oxidized sulfenic acid form (SOH) of the sulfhydryl side chain and the S-glutathionylated intermediate (SSG) initiate changes in protein function, thus effecting the redox signal [22]..... 7
- Figure 1-3:** Current versus time in a chronoamperometric experiment. Current, I_{da} , is normalized by the area, A , of the working electrode in m^2 . The inverse dependence of I_{da} on πt , where t is time in seconds, is seen here. 11
- Figure 2-1:** Detail of 8-TRK probe used in this project (CenMeT, University of Kentucky), with electrode dimensions and spacing. Image and text from [49]. 18
- Figure 2-2:** Setup of probe during calibration. The magnetic stirrer ensured a continuous flow of H_2O_2 to the electrode surface..... 21
- Figure 2-3:** Setup of probe during chronoamperometry experiments (+0.7 V vs. Ag/AgCl reference electrode). Data are recorded at a frequency of 10 Hz and displayed in real time as current (nA) vs. time (sec). 22
- Figure 3-1:** Screenshot of FAST system data obtained during calibration. The x- and y-axes signify, respectively, runtime in minutes:seconds of the ongoing test and current (nA) generated at the microelectrodes. Each colored, horizontal line on the graph represents current generated at one Pt microelectrode. The first H_2O_2 addition is shown near the edge of the figure. 25
- Figure 3-2:** Calibration of probe in the presence of H_2O_2 . A. Increasing volumes of 2 mM H_2O_2 were added at sixty-second intervals such that the following final concentrations were reached: 0 μM , 0.31 μM , 1 μM , 2 μM , 4 μM , 8 μM , and 10 μM . B. A linear fit of the current detected at each calibration step yielded a sensitivity of 6.743 pA/ μM ($R^2 = 0.9979$). 26

Figure 3-3: Effect of lipopolysaccharides (LPS) on hydrogen peroxide production in RAW 264.7 cells. Cells were seeded in 24-well cell culture plates at a density of 1×10^5 cells/well. Upon reaching 40-50% confluency, treated cells were spiked with LPS in two concentrations (200 ng/mL and 500 ng/mL, in triplicate), then incubated for 24 hours. After calibration of the Pt-MEA against H_2O_2 in complete cell culture medium (DMEM), amperometry was performed in each well for four minutes with a potential step of +0.7 V against an Ag/AgCl reference electrode. The sensitivity obtained during calibration (9.975 pA/ μ M; $R^2 = 0.9995$) was used to translate current for each experimental condition to normalized H_2O_2 concentration (μ M). Data shown correspond to Electrode 1 (E1), the electrode nearest the cells. One-way ANOVA ($n = 5$, $p = 0.002$) was performed to assess the significance of differences among all group mean concentrations, followed by the Tukey-Kramer test to assess pairwise significant differences ($n = 5$, $*p < 0.05$, $**p < 0.001$). 30

Figure 3-4: Effect of lipopolysaccharides (LPS) concentration on hydrogen peroxide production in RAW 264.7 cells. Four concentrations of H_2O_2 (200 ng/mL, 500 ng/mL, 800 ng/mL and 1000 ng/mL) were added to cells in triplicate. Cells were incubated 12 or 24 hours. The sensitivity obtained was 4.10 pA/ μ M ($R^2 = 0.9995$). Data shown correspond to Electrode 1 (E1), the microelectrode nearest the cells. One-way ANOVA ($n = 14$, $p < 0.001$) and the Tukey-Kramer test ($n = 14$, $*p < 0.05$, $**p < 0.001$) were used to assess statistical significance..... 32

Figure 3-5: Effect of incubation time on hydrogen peroxide production in RAW 264.7 cells. 200 ng/mL LPS was added to cells plated in triplicate in 24-well plates (seeding density: 1×10^5 cells/mL). Cells were incubated 6, 12, 24 or 48 hours. Probe sensitivity: 11.0 pA/ μ M ($R^2 = 0.9997$). One-way ANOVA ($n = 21$, $p < 0.001$) and the Tukey-Kramer test ($n = 21$, $*p < 0.05$, $**p < 0.001$) were used to assess statistical significance. 33

Figure 3-6: Effect of reduced incubation temperature on H_2O_2 production in RAW 264.7 cells. LPS-doped cells received 200 ng/mL in each well. Cells were incubated for 48 hours at 4 °C or 37 °C (5% CO_2) following addition of LPS. Probe sensitivity: 11.0 pA/ μ M; R^2 , 0.9997. One-way ANOVA ($n = 8$, $p < 0.001$) and the Tukey-Kramer test ($n = 14$, $*p < 0.05$, $**p < 0.001$) were used to assess statistical significance. 34

Figure 3-7: Effect of dexamethasone on H_2O_2 production in RAW 264.7 cells. Cells received 200 ng/mL LPS and/or 200 nM or 400 nM Dex in each well. Cells were incubated for 6, 12, 24, or 48 hours following addition of LPS and/or Dex. Probe sensitivity: 11.0 pA/ μ M; R^2 , 0.9997. One-way ANOVA ($n = 14$, $p < 0.001$) and the Tukey-Kramer test ($n = 14$, $*p < 0.05$, $**p < 0.001$) were used to assess statistical significance. 35

Figure 3-8: Effect of cell culture plate type on H₂O₂ production in RAW 264.7 cells. 6-well, 12-well, and 24-well plates were seeded with RAW 264.7 cells, grown to 40-50% confluency, and incubated with 200 ng/mL LPS for 24 hours. Probe sensitivity: 5.803 pA/μM; R², 0.9985. One-way ANOVA (n = 8, p < 0.001) and the Tukey-Kramer test (n = 14, *p < 0.05, **p < 0.001) were used to assess statistical significance. 36

Figure 3-9: Effect of LPS or ROS probe operation on viability of RAW 264.7 cells. 96-well plates were seeded with 1×10^4 RAW 264.7 cells, grown to 50% confluency, and doped with 200 ng/mL or 500 ng/mL LPS, or probed at one of two potential steps: +0.7 V and +0.3 V. One-way ANOVA (n = 6, p = 0.0029) and Tukey-Kramer post-hoc analysis (n = 6, *p < 0.05, **p < 0.001) were performed. 38

LIST OF TABLES

Table 3-1: Volume of 2 mM H ₂ O ₂ added during each calibration step, with resultant final concentration of H ₂ O ₂ in 10 mL media.	26
---	----

ACKNOWLEDGMENTS

I thank Dr. Scott Poh for his generosity with his time and wisdom, and for the freedom to make productive mistakes. Thank you for showing me that important work is worth doing well, but need not be boring. I am grateful to Dr. Steve Jones for his years of academic advice and for his rigorous guidance in the classroom on all manner of topics. I thank Dr. Bryant Hollins for cheerfully agreeing to serve on my academic committee, and for his patience. I thank Dr. Rebecca Giorno for the use of her lab and for her excellent, practical suggestions on cell culture and experimental design. Finally, I gratefully acknowledge Dr. Prabhu Arumugam and Chao Tan for their expert technical guidance and collaborative effort throughout this project, and for the use of their equipment.

I thank Yashwanthi Yanamadala for her patience and good humor in the trenches. I thank my mentor, Jolin Rodrigues, for her invaluable training in hard and soft skills, her superlative eye for detail, and her steadfast friendship.

CHAPTER 1

INTRODUCTION

1.1 Oxidative Stress

1.1.1 Introduction

Reactive oxygen species (ROS)—principally superoxide ($\bullet\text{O}_2^-$), radical hydroxyl ion ($\bullet\text{OH}$), and hydrogen peroxide (H_2O_2)—are present in nearly all aerobic cell types [1]. Together with reactive nitrogen species (RNS), e.g., nitric oxide ($\bullet\text{NO}$), ROS may transiently exceed the capacity of the body to remove them—a condition known as oxidative stress [2]. Oxidative stress is associated with numerous ill health effects [1–3]. At the cellular level, these ill effects include irreversible oxidation of DNA, lipids, and amino-acid side chains (e.g., protein carbonylation) [1]. Yet biological systems employ ROS/RNS in essential functions, such as the activation of macrophages to deploy ROS in fighting infection [5]. This ROS-mediated “respiratory burst” is a key component of the inflammatory response (see Figure 1-1).

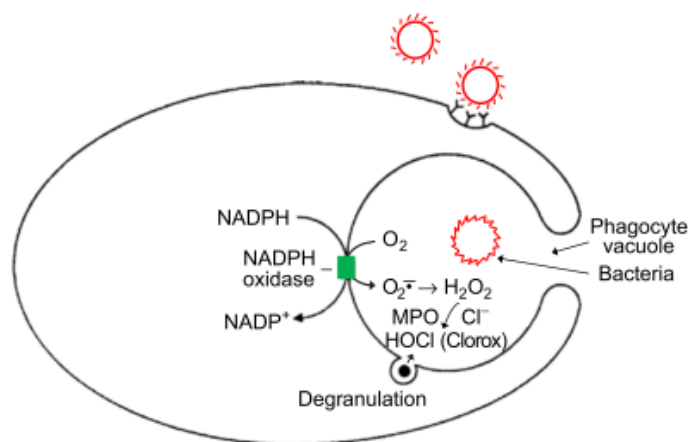


Figure 1-1: Image from Kalyanaraman, B. [2]. Engulfing and oxidation of bacteria by an activated macrophage. In this example of respiratory burst, superoxide anions oxidize microbes directly, while also dismutating to O₂ and H₂O₂. H₂O₂ also reacts with chloride anions to form hypochlorite (HOCl), a potent microbicidal oxidant.

1.1.2 Oxidative Stress and Inflammation

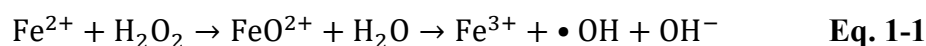
Despite the short-term benefit of this immune response, chronic inflammation is linked to diseases such as cancer, atherosclerosis, rheumatoid arthritis, Parkinson's disease, and Alzheimer's [1, 2, 4, 5]. Chronic inflammation involves a state of prolonged oxidative stress in which the normal mechanisms of inflammatory resolution are impaired or do not function (see M2 macrophages, below) [6]. Chronically elevated levels of ROS, then, may have far-reaching detrimental effects in the body [7].

1.1.3 ROS and Reduction Potential

The standard reduction potential is a measure of the ability of a chemical species at standard state to oxidize a standard hydrogen electrode (SHE) at 298 K [8]. Greater reduction potentials indicate a more robust ability to be reduced, i.e., to gain electrons. Hence, species with more positive reduction potentials are more oxidizing [9].

Most ROS and RNS derive their chemical potency from the presence of highly reactive free radicals, which give these species a range of relatively high reduction

potentials [1, 2]. Many nonradical ROS, while less reactive than radical ROS, are easily converted to a more reactive, radical species [1]. For example, H₂O₂ has a reduction potential of +0.34 V at standard state. When H₂O₂ is produced in, e.g., the phagosome, it may diffuse freely through the phagosomal membrane into the cytosol (or proceed further, to the extracellular environment) [10]. This H₂O₂ oxidizes free cytosolic or enzyme-bound ferrous iron—including, e.g., iron associated with DNA—in a two-step reaction known as the Fenton reaction (see Equation 1-1) [10]. H₂O₂ then decays into the highly reactive radical hydroxyl ion (•OH), which has a reduction potential of +2.33 V [1]:

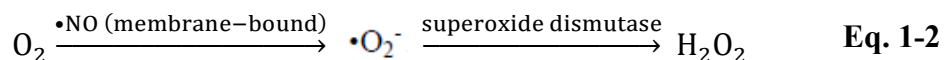


1.2 Overview of Major ROS/RNS

1.2.1 Superoxide (•O₂⁻)

Despite its relatively high one-electron reduction potential (+0.94 V, in contrast to an analogous potential of +0.34 V for H₂O₂) and unpaired electron, superoxide is largely unreactive *in vivo*. The anionic charge of •O₂⁻ is responsible for this relative lack of reactivity: since •O₂⁻ must interact with anion-rich biomolecules such as DNA in order to oxidize them, the activation energy required for such reactions is relatively high [1].

The most prevalent sources of endogenous superoxide are the electron transport chain of mitochondria—which generates superoxide radicals and occasionally hydrogen peroxide—and transmembrane NADPH oxidase (NOX) complexes, which generate superoxide radicals outside the cell (see Equation 1-2, adapted from [3]).



As mentioned above, superoxide production *in vivo* leads to downstream production of more toxic ROS (e.g., radical hydroxyl ion). In mitochondria, superoxide is continuously generated *in vitro* at rates of 1-2% of the total molecular oxygen consumed by Complexes I and III of the electron transport chain [1]. Additionally, the radical species ubiquinone (i.e., Coenzyme Q, ubiquinone, in its one-electron reduction state) provides electrons to O₂, generating superoxide [11].

Because these processes are intrinsic to aerobic respiration, the scavenging enzyme superoxide dismutase (SOD) is essential to host defense in aerobic organisms (see Equation 1-2) [12]. In *E. coli*, mutants lacking SOD exhibit growth defects in aerobic conditions, while growth in anaerobic environments is unaffected [13].

1.2.2 Radical Hydroxyl Ion (•OH)

Hydroxyl radicals are generated exogenously by ionizing radiation (e.g., in the treatment of cancer) [1, 2]. Within the body, the reduction of hydrogen peroxide in the presence of ferrous iron produces hydroxyl radicals as a byproduct (see the Fenton reaction, Equation 1-1, above) [12]. The hydroxyl radical ion is an “indiscriminately toxic” oxidant in physiological systems [2]. Its second-order rate constant ($7 \times 10^9 \text{ M}^{-1} \text{ s}^{-1}$) in the oxidation of free methionine is two orders of magnitude greater than that of hypochlorous acid (i.e., bleach) and eleven orders of magnitude greater than that of hydrogen peroxide [14]. In effect, hydroxyl radicals oxidize the first biomolecular target available—e.g., proteins, nucleic acids, or lipids—with the rate of reaction limited only by diffusion [14].

1.2.3 Nitric Oxide (\bullet NO)

\bullet NO relaxes smooth muscle in vascular endothelium, dilating the associated blood vessels and causing a subsequent drop in blood pressure [15]. This benign effect is achieved through direct interaction of \bullet NO with the heme cluster in guanylyl cyclase, which catalyzes production of cyclic guanine monophosphate (cGMP) from cyclic guanine triphosphate (cGTP) [15].

The biosynthesis of \bullet NO from L-arginine and oxygen is catalyzed by any of three isoforms of nitric oxide synthase (NOS): neuronal NOS (nNOS), endothelial NOS (eNOS), and inducible NOS (iNOS) [16]. nNOS-derived \bullet NO, in addition to its vasodilatory, hypotensive effect in the central (CNS) and peripheral (PNS) nervous systems, mediates long-term synaptic plasticity in the CNS [16]. eNOS-derived \bullet NO aids in vasodilation and vasoprotection throughout the body. This vasoprotective role arises from the anti-atherogenic effect of \bullet NO: nitric oxide prevents the transcription of several factors that aid in plaque formation in the vascular lumen [16].

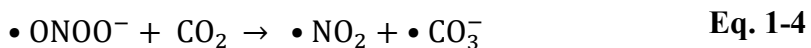
iNOS is released by pro-inflammatory (M1) macrophages dispatched to fight infection or injury (see the subsection on inflammation, below). This NOS isoform plays a critical role in the inflammatory response: large quantities of iNOS-derived \bullet NO function as a local, bactericidal oxidant (in concert with other ROS, e.g. H_2O_2) [16].

Under inflammatory conditions, \bullet NO reacts with $\bullet\text{O}_2^-$ to form the non-radical RNS peroxynitrite (ONOO^- ; see Equation 1-3) [17].



Peroxynitrite is itself a damaging oxidant, but its rate of reaction with biomolecules is slower than, e.g., superoxide anion [1]. However, peroxynitrite reacts

with carbon dioxide (CO₂) to form nitrogen dioxide (•NO₂) and the highly reactive radical carbonate anion (•CO₃⁻; see Equation 1-4) [18].



Here again is an example of a non-radical, somewhat reactive species converted to a more damaging, radical oxidant.

1.2.4 Hydrogen Peroxide

Hydrogen peroxide is a non-radical product of the SOD-catalyzed dismutation of superoxide, which is produced continuously in mitochondria and elsewhere (see Equation 1-2, above). The two-electron reduction of hydrogen peroxide is more thermodynamically favorable than that of hypochlorous acid (bleach), implying an even greater oxidative capacity [19]. However, in physiological conditions, the activation energy of the two-electron reduction is prohibitively high. This kinetic constraint allows hydrogen peroxide to diffuse freely through cell membranes without directly oxidizing cellular components [19]. Much of the oxidative damage caused by hydrogen peroxide occurs indirectly, e.g., through the Fenton reaction in the presence of ferrous iron and the subsequent production of hydroxyl radicals (see Equation 1-2, above) [20].

Hydrogen peroxide is the primary courier of redox signals in the body [21]. The diverse array of signaling functions regulated by H₂O₂ is largely achieved through oxidation of ionized thiol (thiolate, S⁻) groups—principally, low-pK_a cysteine (Cys) residues in redox-sensitive proteins (see Figure 1-2; [22]).

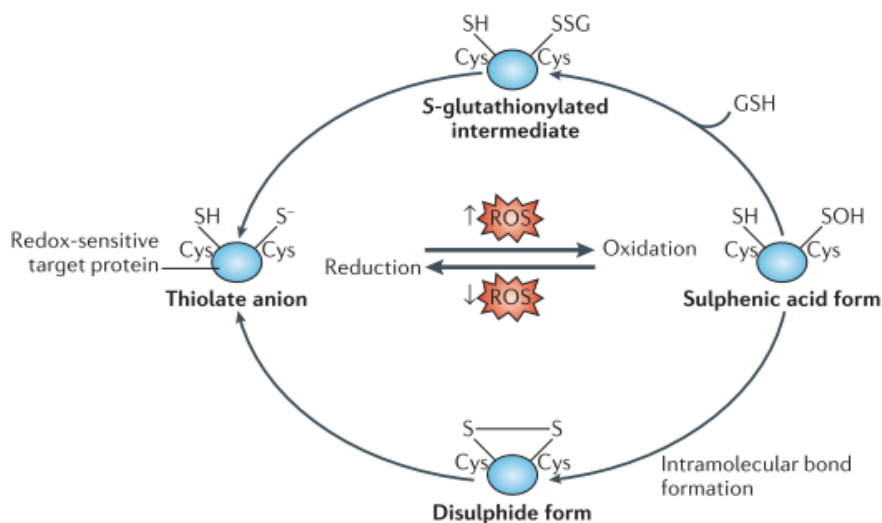


Figure 1-2: Redox cycling of two cysteine (Cys) residues within a redox-sensitive target protein (image from [22]). The H_2O_2 -oxidized sulphenic acid form (SOH) of the sulfhydryl side chain and the S-glutathionylated intermediate (SSG) initiate changes in protein function, thus effecting the redox signal [22].

1.3 Role of Macrophages in Inflammation

1.3.1 Overview

Inflammation, a complex set of physiological responses to tissue infection or injury, may be acute or chronic; local or systemic; endogenously or exogenously induced [6]. Acute inflammatory episodes consist of two phases: 1) inflammation and 2) resolution.

Fixed, tissue-resident macrophages comprise the first line of defense against infection or tissue injury [15]. In the case of, e.g., acute *E. coli* infection, lipopolysaccharides (LPS) present on the outer membrane of the bacteria bind to Toll-Like Receptors (TLRs) of tissue macrophages, whereupon, as part of a cascade of rapid inflammatory responses, capillaries near the site of infection are rendered selectively permeable to circulating neutrophils [6]. Some of these neutrophils enter the

extravascular space and degranulate, releasing highly bactericidal (and cytotoxic) ROS. Other neutrophils engulf bacteria through phagocytosis [6].

If the invading pathogens are not destroyed by neutrophils, activated macrophages proceed by chemotaxis to the site of infection, engulfing large numbers of bacteria and releasing lethal quantities of ROS/RNS in the so-called respiratory burst [15].

Thus, elevated ROS/RNS are a hallmark of inflammation and oxidative stress [2]. Since H_2O_2 is the most stable ROS *in vivo*, H_2O_2 is a suitable choice of biomarker in an assay of inflammation [19].

1.3.2 The M1/M2 Paradigm of Macrophage Polarization

Macrophages activated by infectious agents (e.g., LPS), pro-inflammatory cytokines (e.g., interferon gamma; $IFN-\gamma$), or injury take on a pro-inflammatory character. These M1 macrophages synthesize iNOS, which catalyzes the synthesis of $\bullet NO$ from L-arginine. $\bullet NO$ is a precursor to more reactive RNS, such as $ONOO^-$ [23]. M1 macrophages fight infection through the production of pro-inflammatory cytokines (e.g., tumor necrosis factor α ; $TNF-\alpha$), the release of ROS/RNS at the site of injury, and the phagocytosis of invading bacteria [24].

In a first step toward resolution of inflammation, local release of anti-inflammatory cytokines such as interleukin 4 (IL-4) modifies the behavior of tissue macrophages near the ongoing inflammatory phase. These M2-polarized macrophages express the enzyme arginase, shunting arginine-derived nitrogen away from the nitric oxide synthesis pathway and toward synthetic processes that aid in the walling-off of pathogens and rebuilding of tissue [23]. Thus, macrophages are crucial mediators of every stage of the inflammatory process.

1.3.3 Professional Phagocytes and the Respiratory Burst

Each of the three types of so-called professional phagocytes—monocytes, neutrophils, and macrophages—responds to microbial infection (i.e., LPS activation) by producing large quantities of NADPH oxidase (NOX2)-derived $\bullet\text{O}_2^-$ within the phagosome [21, 22]. Spontaneous or SOD-catalyzed dismutation of this $\bullet\text{O}_2^-$ occurs, leaving H_2O_2 free to diffuse through the phagosomal and plasma membranes into the extracellular space [27].

1.3.4 Selection of Cell Line for This Project

Thus, possible choices of cell type for this research included each of the three professional phagocytes: monocytes, neutrophils, and macrophages each produce NOX2-derived $\bullet\text{O}_2^-$ (i.e., indirectly, H_2O_2) at different stages of pathogen-induced inflammation [25].

However, monocytes and neutrophils must be induced from peripheral blood mononuclear cells (PBMCs), which themselves must be isolated by density gradient centrifugation from whole blood samples [28]. Upon induction of these phenotypes, monocytes and neutrophils are difficult to culture continuously. Thus, only macrophages are readily available as conveniently cultured, quickly dividing, continuous cell lines.

Of the available macrophage cell lines, the murine macrophage-like cell line RAW 264.7 is among the most widely used [29]. RAW 264.7 cells were derived from functional macrophages isolated from a virus-induced tumor in mice [30]. They are functionally and genetically stable through at least 18 and up to 50 passages [29]. They are well-studied with respect to LPS-induced production of ROS [25-27].

RAW 264.7 cells are conveniently maintained in culture: they require no more than one media change between passages. They divide rapidly: throughout this project, 24-well plates seeded with 1×10^5 cells per well reached 50% confluency in 24 hours.

1.4 Chronoamperometry

Chronoamperometry is an electroanalytical method in which a square potential step is applied between the working and reference electrodes in an electrochemical cell [9]. In an unstirred bulk solution with rapid reduction (or oxidation) occurring at the working electrode, the Faradaic current produced in the working electrode depends on the rate of diffusion of the analyte (e.g., H_2O_2) toward the electrode surface and on time [9]. For a planar electrode, the time-dependent current $I(t)$ is given by the Cottrell equation:

$$I(t) = nF a c_R \sqrt{\frac{D_R}{\pi t}} \quad \text{Eq. 1-5}$$

where n is the number of electrons, F is the Faraday constant, a is the area of the planar electrode (cm^2), c_R is the initial concentration of the analyte, D_R is the diffusion coefficient of the analyte (cm^2/s), and t is time (sec) [9].

A typical chronoamperometric plot of current vs. time is seen in Figure 1-3 [9]:

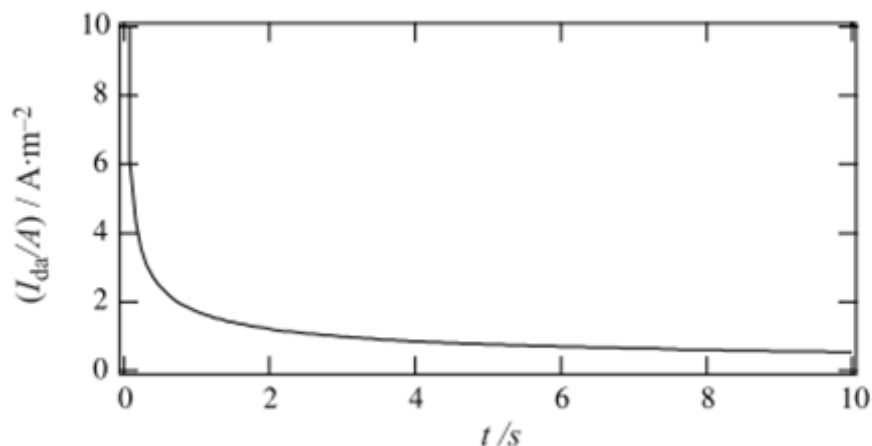


Figure 1-3: Current versus time in a chronoamperometric experiment. Current, I_{da} , is normalized by the area, A , of the working electrode in m^2 . The inverse dependence of I_{da} on $\sqrt{\pi t}$, where t is time in seconds, is seen here.

1.4.1 Use of Chronoamperometry in Industrial Detection of Hydrogen Peroxide

H_2O_2 is used extensively in the treatment of domestic and industrial wastewater [31]. The ability of H_2O_2 to oxidize aqueous and organic pollutants is exploited in these applications: for example, Fe_2SO_4 is used to generate Fe^{2+} , which, in combination with H_2O_2 , yields the Fenton reaction (i.e., generation of $\bullet OH$; see Equation 1-1, above) and subsequent oxidation of fecal coliforms present in domestic waste [32]. Such applications require frequent determination of H_2O_2 . Amperometric platinum (Pt) electrodes with various surface modifications have been used for this purpose [31].

1.4.2 Use of Chronoamperometry in Real-Time Detection of H_2O_2 Release

Amatore et al. (2007) first reported the use of chronoamperometry in the detection of H_2O_2 produced by RAW 264.7 cells placed under oxidative stress [33]. Approximately twenty RAW 264.7 cells were cultured within a microfluidic chamber containing two Pt band microelectrodes and an Ag/AgCl reference electrode.

In order to simulate the oxidative burst present in inflammation, a calcium ionophore that rapidly depolarizes the cell membrane was injected into the chamber. The

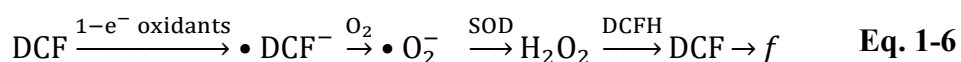
resulting release of H₂O₂ was detected in real time as a sharp increase in current above baseline: current peaked at approximately 180 seconds and reverted to baseline 600 seconds after injection of the ionophore [33].

1.5 Project Overview

1.5.1 Typical Methods of ROS Detection

1.5.1.1 Intracellular Methods

Intracellular methods of H₂O₂ detection are predominantly fluorescence-based [34]. Among the most popular of these is dichlorodihydrofluorescein diacetate (DCFH-DA). Upon diffusion into the cell, DCFH-DA is deacetylated to form a membrane-impermeable product: DCFH [34]. In the presence of H₂O₂, DCFH undergoes a two-electron oxidation to form a fluorescent product, dichlorofluorescein (DCF); however, this reaction is not direct and DCF:H₂O₂ stoichiometry is not 1:1 [17]. DCF fluorescence is often erroneously reported as a direct measure of intracellular H₂O₂ generation, yet numerous other oxidative pathways to this product have been documented in the literature [34]. For example, •O₂⁻ generated by the one-electron oxidation product of DCF may artificially increase intracellular H₂O₂, yielding increased fluorescence as an artifact (see Equation 1-4, adapted from [34]):



where f is fluorescence emission.

A variety of more H₂O₂-specific, fluorescence-based intracellular assays exploit the strong propensity of H₂O₂ to oxidize boronate groups into corresponding phenols [35]. These boronate-deprotection assays show greater specificity and customizability

(e.g., they may be targeted to specific organelles such as mitochondria), but they are unreliable as quantitative assays of H₂O₂ production [35].

1.5.1.2 Extracellular Methods

The Amplex Red reagent (Thermo Fisher) is commonly used as an extracellular indicator of H₂O₂ production. Amplex Red is oxidized by horseradish peroxidase (HRP) in the presence of H₂O₂ to form resorufin, a fluorogenic molecule [34]. This assay is highly specific for H₂O₂ and, because H₂O₂:resorufin stoichiometry is 1:1, may be used to quantify extracellular H₂O₂ production [34]. However, like all fluorescent molecules, resorufin is subject to photobleaching and subsequent attenuation of fluorescence. This tendency presents a practical problem in the design of an assay of inflammation.

1.5.2 Project Rationale

As discussed above, the use of chronoamperometry in the detection of H₂O₂ and other ROS/RNS released by a small population of RAW 264.7 cells in a Pt MEA-containing microfluidic chamber has been demonstrated [33]. However, the intricacy of such a design may be of limited utility in a medical laboratory.

On the other hand, the ready availability of flexible, ceramic, Pt MEA probes may permit the development of a more scalable assay of extracellular H₂O₂. Furthermore, the ease of modifying the microelectrode surface allows for a wide range of multiplexed applications: Hossain et al. report the fabrication of a multiplexed glutamate/gamma-aminobutyric acid (GABA) probe via the addition of glutamate oxidase (GLOX) and GABase to separate microelectrodes within the same probe; this probe was used to detect *ex vivo* release of GABA in hippocampal rat brain slices [36]. Scoggin et al. report the

use of GIOX-modified probes *in vitro* to detect glutamate uptake in astrocytes versus glioma cells [37].

Oxidative stress and inflammation play a central role in numerous disease pathways. In rheumatoid arthritis (RA), for example, an autoimmune disorder causes activated macrophages, neutrophils, and other immune cells to attack synovial joints [38]. For the patient, this disease manifests as a progressive, relapsing inflammation of the synovial lining with attendant swelling, stiffness and pain [39]. Blood samples drawn from patients with RA exhibit increased lipid peroxidation, protein carbonylation, DNA damage, and ROS/RNS [38]. The synovial fluid of RA patients is marked by increased levels of inflammation-associated cytokines (e.g., TNF- α), transcription factors (e.g., nuclear factor- κ B), $\bullet\text{O}_2^-$, and $\bullet\text{NO}$ [40]. Furthermore, synovial fluid in RA patients contains reduced levels of antioxidants and oxidant-scavenging enzymes [36].

For a hypothetical RA patient in an early stage of the disease, a multiplexed OS assay might detect elevated $\text{H}_2\text{O}_2/\bullet\text{NO}$ in synovial fluid or blood before the onset of chronic symptoms. Since early intervention in RA is associated with successful outcomes, such a preventive approach in high-risk patients might be beneficial [35]. Additional modifications to the probe would permit simultaneous monitoring of the disease state and the progress of molecular or enzymatic antioxidant therapy.

Inflammation is essential to the development of cardiovascular disease [41]. Atherogenesis depends on the chemokine-driven recruitment of monocytes to the site of lesions in the vascular endothelium. These monocytes then differentiate into pro-inflammatory macrophages that engulf lipoproteins, including ROS-oxidized low density lipoproteins (Ox-LDL) [42]. Lipid-loaded macrophages, in turn, become foam cells,

which may become apoptotic and seed a core of necrotic cells within atherosclerotic plaques [41]. This necrotic core (NC) may spread throughout the plaque, causing detachment of the plaque from the endothelium and creating the risk of an embolism or ischemic stroke [39]. An even more acute risk of atherosclerosis with NC is plaque rupture. This condition is responsible for “~70% of fatal acute myocardial infarctions and/or sudden coronary deaths” [43]. In part, plaque instability is yet another consequence of oxidative stress: ROS aid in the release of matrix metalloproteinases (MMPs) that physically weaken the vascular basement membrane and plaque surface [44]. In the event of plaque rupture, a coronary thrombus may be ejected into the arterial lumen. Plaque rupture-derived coronary thrombosis is the direct cause of most myocardial infarctions [43].

Because oxidative stress and atherosclerosis are highly correlated, a preventive strategy, as outlined above, would give at-risk patients an opportunity to address lifestyle risk factors (e.g., smoking) before the onset of chronic symptoms [39]. By detecting chronic oxidative stress in its early stages, a multiplexed ROS/RNS assay administered at the point of care would aid in such a strategy.

Non-fluorescent extracellular methods employed to detect oxidative stress are indirect: they quantify already-existing oxidative damage (e.g., detection of lipid peroxidation). Thus, the need for a direct, extracellular, robust assay of ROS has not yet been addressed: Brenner et al. write that there are “no standardized methods to capture actual ROS levels in humans to date” [45]. The aim of this research is to develop such an assay.

The immediate goal of this project is the post-hoc detection of stable concentrations of H₂O₂ released by a large population of macrophages. Hence, real-time detection of H₂O₂ production by a small population of cells, as in Reference 31, was not attempted. Instead, H₂O₂ release was induced as follows: 1×10^5 RAW 264.7 cells were incubated with varying concentrations of LPS for 6-48 hours before testing for 4-8 minutes with the probe (see Methods, below). This protocol was broadly similar to previous studies exploring ROS/RNS released by RAW 264.7 cells [25-27].

To assess the feasibility of the Pt MEA as an ROS assay, the following hypotheses were tested:

1. The probe will sense H₂O₂ over a physiologically relevant linear range.
2. RAW 264.7 cells will produce H₂O₂ in response to LPS doping.
3. The probe will detect significantly more H₂O₂ in LPS-doped samples than in untreated controls (i.e., the H₂O₂ produced will be stable in culture medium).
4. LPS-stimulated H₂O₂ production will be greater at 37 °C than at 4 °C.
5. Dexamethasone will attenuate H₂O₂ production in LPS-doped samples.
6. LPS doping and the operation of the probe will not adversely affect cell viability.

CHAPTER 2

METHODS

2.1 Fabrication and Preparation of Pt MEA Probes

2.1.1 Fabrication

All Pt MEA probes were fabricated at the Center for Microelectrode Technology (CenMeT, University of Kentucky) in conjunction with Thin Film Technology, Inc. (Buellton, CA). Fabrication was performed as follows: a ceramic wafer (0.005 ± 0.0005 in. thick) was cleaned with sulfuric acid and chromium trioxide, rinsed with deionized water, and dried at 120 °C [48]. Photoresist was evenly spun over the whole surface of the ceramic wafer. A mask was used to etch the design of the microelectrode recording sites, bonding pads, and wires onto the photoresist [48]. Upon development of the photoresist, this design was exposed. An adhesion layer of titanium (500 Å), followed by the layer of platinum (1500 Å) that would comprise the Pt MEA, was coated onto the printed circuit [48]. Each ceramic wafer contained 56 microelectrodes. Upon diamond cutting of the wafer into discrete probes, each new probe contained eight platinized, platinum microelectrodes ($100 \mu\text{M} \times 50 \mu\text{M}$) in four pairs (see Figure 2-1).

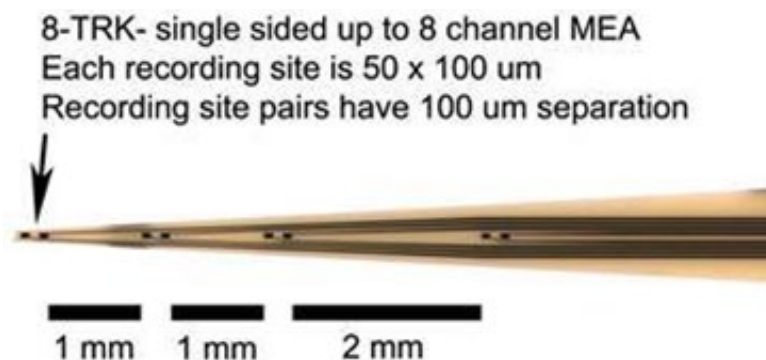


Figure 2-1: Detail of 8-TRK probe used in this project (CenMeT, University of Kentucky), with electrode dimensions and spacing. Image and text from [49].

2.1.2 Cleaning

The probes were acid-cleaned and coated with mPD in collaboration with the laboratory of Dr. Prabhu Arumugam.

The Pt MEA probe was immersed in 0.05 M sulfuric acid in a two-electrode setup. In lieu of the Ag/AgCl reference electrode used in ROS assays, the more robust saturated calomel electrode (SCE) was used.

A potentiostat (Gamry) was used to cycle one Pt microelectrode 15 times between -0.3 V and $+1.0$ V with a scan rate of 20 mV/s. Each of the remaining microelectrodes was cycled in this manner.

2.1.3 Application of MPD Layer

The Pt MEA was immersed in a nitrogen-purged, 10 mM solution of mPD in 1 M NaCl. The same Pt MEA/SCE two-electrode setup described above was used, and each of the microelectrodes was continuously cycled between $+0.2$ V and $+0.8$ V, with a scan rate of 50 mV/s, for 40 mins. Upon completion of potential cycling, the probe was rinsed with deionized water and allowed to air dry overnight.

2.2 Cell Culture

2.2.1 Maintenance of Cells in Culture

RAW 264.7 cells (American Type Cell Collection) were maintained in Dulbecco's Modified Eagle's Medium (DMEM; VWR) with 4.5 g/L glucose, L-glutamine, and sodium pyruvate, supplemented with 10% FBS and 1% penicillin/streptomycin. Cells were cultured in 75 cm² cell culture flasks (CellStar; T-75) and grown in a 37 °C, 5% CO₂ incubator (VWR). Media was changed every 2-3 days or as needed: flasks were checked daily for notable color changes in the media. A pinkish-orange appearance indicated acidification by cellular waste products of the phenol red pH indicator present in DMEM.

When the cells reached 80% confluency, 13 mL of DMEM were aliquoted to a new T-75 flask and allowed to equilibrate for ten minutes in the CO₂ incubator. Meanwhile, the cells were harvested via scraping and resuspension in 4 mL DMEM. 400 µL of this cell suspension were transferred to the new flask, which was returned to the incubator.

2.2.2 Plating of RAW 264.7 Cells

After the harvested cells were resuspended (see previous subsection) in 4 mL DMEM, the cell suspension was transferred to a 15 mL tube (Corning) and vortexed at speed setting 7 on a VWR vortexer. The cell suspension was diluted 1:4 in DMEM. 20 µL of this cell suspension was mixed with 20 µL trypan blue (for the visualization of dead cells). 10 µL of this mixture were added to both counting chambers of a Reichert Bright Line hemocytometer (Hausser). Cells were visualized at 10X magnification on an inverted light microscope (Olympus) and checked for an abnormally high (>5%)

proportion of dead cells, then counted (one large square per counting chamber). The average cell count was used to obtain the concentration in cells/mL of the original cell suspension.

The cell suspension was vortexed and a portion of the cells diluted in DMEM to a concentration of, e.g., 1×10^5 cells/mL (for other plate types, seeding density was scaled up or down according to the surface area of the plate wells). In 24-well plates, 1 mL of cell suspension was aseptically added to the appropriate number of wells.

2.3 Treatment of Cells with Lipopolysaccharide (LPS) or Dexamethasone

After 24 hours, the confluency of the cells was assessed under the inverted light microscope. When the cells were 50% confluent, they were doped with lipopolysaccharides (LPS) and/or dexamethasone (Dex) and placed in the incubator.

RAW 264.7 cells were stimulated with varying concentrations of LPS (Enzo LifeSciences) derived from *Escherichia coli* strain EH100 (Ra mutant). Cells were also treated with varying concentrations of dexamethasone (Alfa Aesar; Dex). Both reagents were added via one of two methods:

2.3.1 Method 1

Beginning with stock solutions of LPS or Dex and diluting separately in complete DMEM warmed to 37 °C, a 2X working solution of each desired final concentration was prepared. After aspirating spent media from each well, cells received, e.g., for LPS-only groups, 0.5 mL 2X LPS solution and 0.5 mL DMEM.

2.3.2 Method 2

10X working solutions of each desired final concentration of LPS or Dex were prepared in 1X phosphate buffered saline (PBS). 100 μL of media from each well was aspirated and replaced with an equivalent volume of 10X LPS, 10X Dex, or PBS. Wells receiving LPS and Dex had 200 μL media removed and replaced by 100 μL of each of the respective solutions.

2.4 Setup and Use of the Probe

2.4.1 Calibration in the Presence of H_2O_2

An 8-TRK probe was affixed to the head stage, which was connected to the Fast Analytical Sensing Technology (FAST) potentiostat/control box (FAST-16mkIII, Quanteon), and submerged in 10 mL DMEM in a 20 mL beaker (Figure 2-2). A stirring hot plate (Corning) and micro magnetic stir bar were also used to ensure continuous diffusion of H_2O_2 to the Pt MEA surface.



Figure 2-2: Setup of probe during calibration. The magnetic stirrer ensured a continuous flow of H_2O_2 to the electrode surface.

While the media was stirred at a constant rate, amperometry was performed as described below. When the slope of the current readout reached a sufficiently flat baseline ($<|2|$ pA/min), increasing volumes of a 2 mM solution of stabilized H_2O_2 (Sigma) were aliquoted to the beaker and the corresponding increases in current noted. Sensitivity (pA/ μM) was the slope of the calibration curve.

2.4.2 Detection of Extracellular H_2O_2

Each 24-well plate was removed from the incubator and partially immersed in a 37 °C water bath (VWR). The Pt MEA was secured to a manual micromanipulator (World Precision Instruments), which was positioned such that the probe entered the culture medium and remained fixed 5 mm above the bottom surface of the plate (see Figure 2-3).

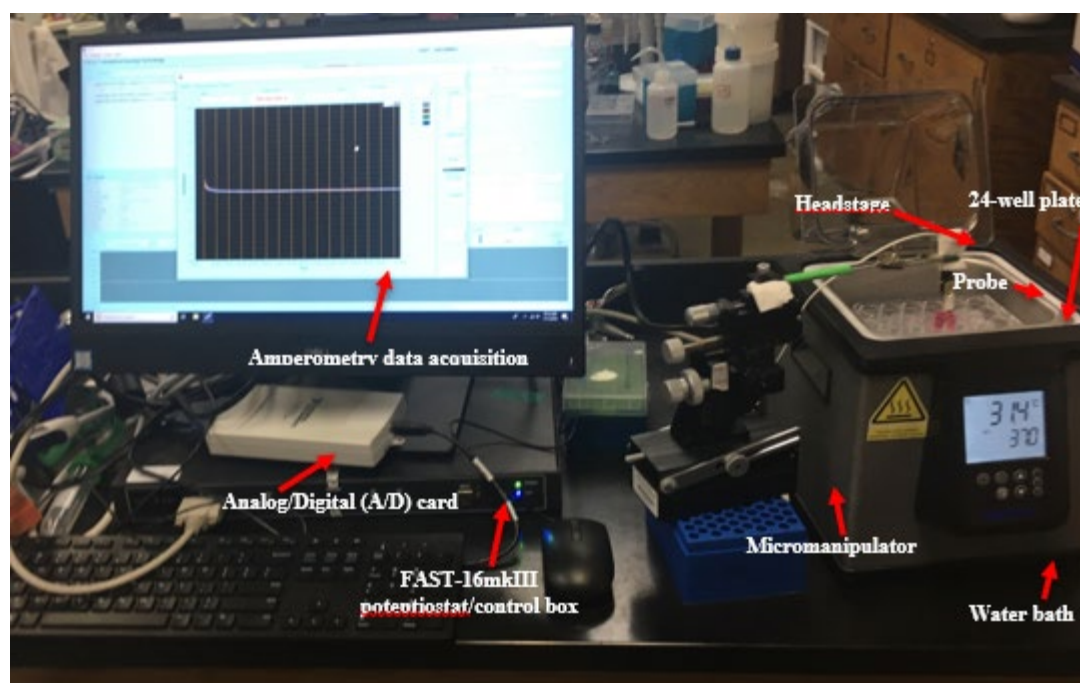


Figure 2-3: Setup of probe during chronoamperometry experiments (+0.7 V vs. Ag/AgCl reference electrode). Data are recorded at a frequency of 10 Hz and displayed in real time as current (nA) vs. time (sec).

Using the mPD-coated platinum microelectrode array (Pt MEA) with the FAST-16mkIII potentiostat in a two-electrode configuration, we performed chronoamperometry at an applied potential of +0.7 V with reference to an Ag/AgCl electrode. Current measurements were taken at a frequency of 10 Hz. The FAST system software (Quanteon) was used in all chronoamperometry experiments.

Prior to each amperometry experiment, the probe was calibrated via the stepwise addition of H₂O₂ to cell culture medium. Abnormally large baseline currents obtained during calibration were assumed to reflect degradation of the mPD coating. Much empirical evidence established that the selectivity of such probes was compromised; 100 pA was selected as the baseline current above which probes should be discarded and replaced.

As proof of concept for detection of H₂O₂ release, RAW 264.7 cells were incubated until they reached 50% confluency, then doped with 200 ng or 500 ng LPS. After further incubation for 24 hours at 37 °C, the cells were probed.

To optimize replicability of this general procedure, two different methods of LPS doping were tested (see below).

RAW 264.7 cells were then doped with four different concentrations of LPS (200 ng/mL, 500 ng/mL, 800 ng/mL, and 1 µg/mL), then incubated 24 hours in order to find the optimal dose for H₂O₂ production. This concentration of LPS (200 ng/mL) was used in the remaining experiments.

Next, doped cells were incubated for 6, 12, 24, or 48 hours in order to discern the effect of post-LPS incubation time on ROS release

To assess the effect of reduced incubation temperature on H₂O₂ production, extracellular H₂O₂ was quantified after incubating LPS-doped cells for 48 hours at 37 °C or 4 °C.

The anti-inflammatory effect of dexamethasone was assessed by repeating the 6/12/24/48-hour experiment (see above) with the addition of Dex (200 nM or 400 nM) in conjunction with LPS.

The effects of well volume and surface area (i.e., cell culture plate type) on H₂O₂ production were then assessed via doping, incubating, and testing cells in 6-, 12-, or 24-well plates.

Finally, an MTT assay (Promokine) was used to determine the effect of LPS or amperometry on cell viability.

CHAPTER 3

RESULTS AND DISCUSSION

3.1 Calibration of the Probe in the Presence of H₂O₂

Chronoamperometry was performed in 10 mL stirred DMEM (+0.7 V voltage step versus Ag/AgCl; scan rate: 1000 Hz; recording frequency: 10 Hz). When a stable baseline current was reached (see Figure 3-1), H₂O₂ was aliquoted into the stirred media at 60-second intervals (see Table 1 and Figure 3-2).

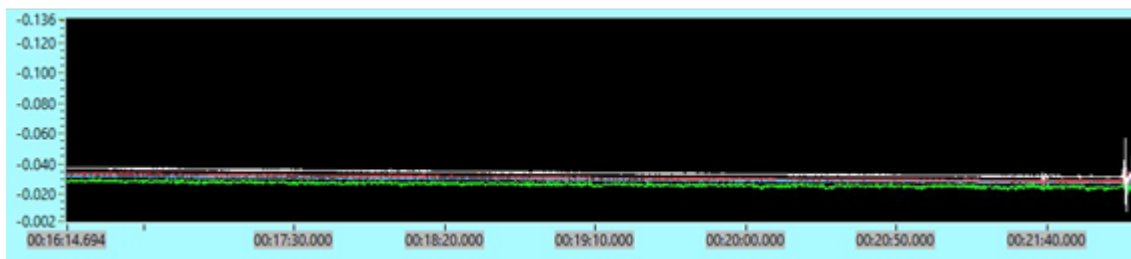


Figure 3-1: Screenshot of FAST system data obtained during calibration. The x- and y-axes signify, respectively, runtime in minutes:seconds of the ongoing test and current (nA) generated at the microelectrodes. Each colored, horizontal line on the graph represents current generated at one Pt microelectrode. The first H₂O₂ addition is shown near the edge of the figure.

Table 3-1: Volume of 2 mM H₂O₂ added during each calibration step, with resultant final concentration of H₂O₂ in 10 mL media.

Step	H ₂ O ₂ added (μL)	[H ₂ O ₂] (μM)
1	1.55	0.31
2	3.45	1
3	5	2
4	10	4
5	20	8
6	10	10

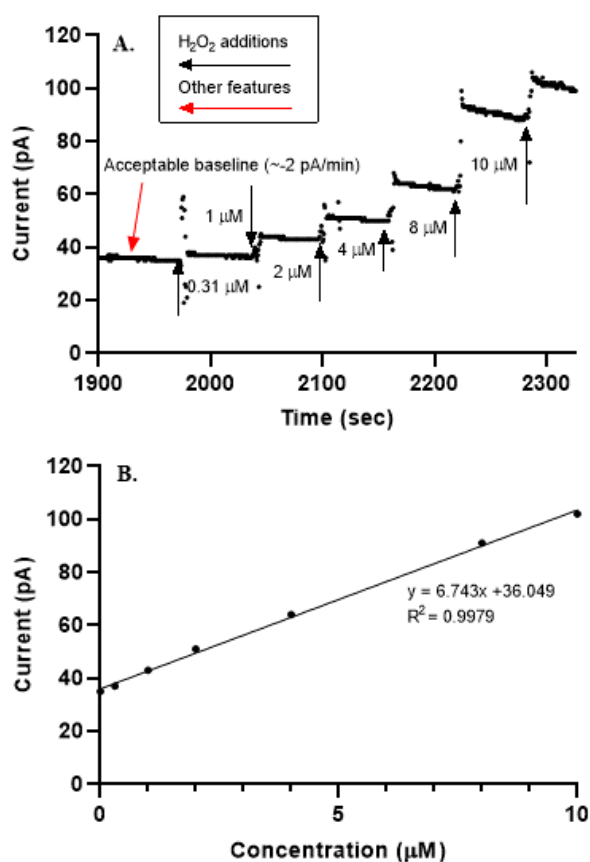


Figure 3-2: Calibration of probe in the presence of H₂O₂. A. Increasing volumes of 2 mM H₂O₂ were added at sixty-second intervals such that the following final concentrations were reached: 0 μM, 0.31 μM, 1 μM, 2 μM, 4 μM, 8 μM, and 10 μM. B. A linear fit of the current detected at each calibration step yielded a sensitivity of 6.743 pA/μM ($R^2 = 0.9979$).

Sources of noise included the stirring of the media; vibrations issuing from the CO₂ incubator; and air currents above the beaker. While it was impracticable to unplug the incubator or test at another location, care was taken to minimize sudden motion near the probe during testing. When manually analyzing calibration data, sudden spikes were disregarded as noise artifacts. The analysis of experimental data was automated in MATLAB; brief, random noise was filtered via the averaging of detected current at fifty evenly spaced times across the last minute of testing. Additionally, the use of cell-free controls in each experiment helped ensure that noise of a longer duration would not artificially increase current.

3.2 Optimization of LPS Doping Protocol

3.2.1 Modification of Method 1

To test the ability of the probe to detect H₂O₂ released by LPS-doped macrophages, 1×10^5 cells/well were seeded in 24-well plates. Previous studies had shown that ROS are reliably detected over a wide range of time points after doping with various concentrations of LPS [51, 55-56]. As a first step toward optimization of LPS concentration and cell confluency prior to LPS addition, 24 hours was selected as a suitable median time point at which to test Method 1. When the cells were 50% confluent, they were doped with 200 ng/mL or 500 ng/mL LPS according to Method 1 (see above), incubated 24 hours, and tested. The following controls were included in this experiment:

Negative controls:

- 1) Media only: 1 mL DMEM was added to empty wells at time of doping. This control provided the background signal to which other groups were normalized.
- 2) Cells only: Wells with media and cells only. Media was changed in this group at time of doping.

Positive controls:

- 1) H₂O₂ (2 mins): 2 μ L of stock H₂O₂ was aliquoted two minutes before testing into wells containing media and cells (final concentration in well: 4 μ M).
- 2) H₂O₂ (24 hrs): 2 μ L of stock H₂O₂ was aliquoted 24 hours before testing (i.e., at the time of LPS addition) to wells containing media and cells. This control was included to ensure that a known concentration of exogenous H₂O₂ would remain stable enough in solution to be detected by the probe. The difference in signal between both positive controls would be used to assess the stability of extracellular H₂O₂ released by LPS-doped cells.

Method 1 showed initial promise, but results proved difficult to replicate. Two potential causes were identified:

1) Changing the entire volume of media at the time of doping might stress the cells to varying degrees, thus producing inconsistent increases in H₂O₂ within a given experiment.

2) Directly diluting small volumes (2-5 μ L) of the LPS stock solution by a factor of 2000 or 5000 may lead to incomplete dilution or loss of the reagent.

To minimize disturbances to the cells, it was decided that the full volume of media should not be aspirated from each well. To ensure that the small volume of stock LPS required was not lost in dilution, the doping protocol was modified to Method 2: LPS was diluted from the stock concentration of 1 mg/mL to a primary working solution of 40 µg/mL in PBS, then diluted again in PBS to a 10X solution of the concentration of interest. These working solutions were added to the relevant wells in 100-µL aliquots.

3.2.2 Proof of Concept – Method 2

To assess the efficacy of this modified doping protocol, the following experiment was performed: RAW 264.7 cells were seeded in 24-well plates as above, incubated 24 hours and doped with 200 ng/mL or 500 ng/mL LPS.

The resulting data showed an enhanced H₂O₂-generating response in LPS-doped cells, with significantly elevated H₂O₂ production in both 200 ng/mL- (p = 0.039) and 500 ng/mL-treated (p = 0.021) cells (see Figure 3-3). H₂O₂ produced was not significantly different between the two groups.

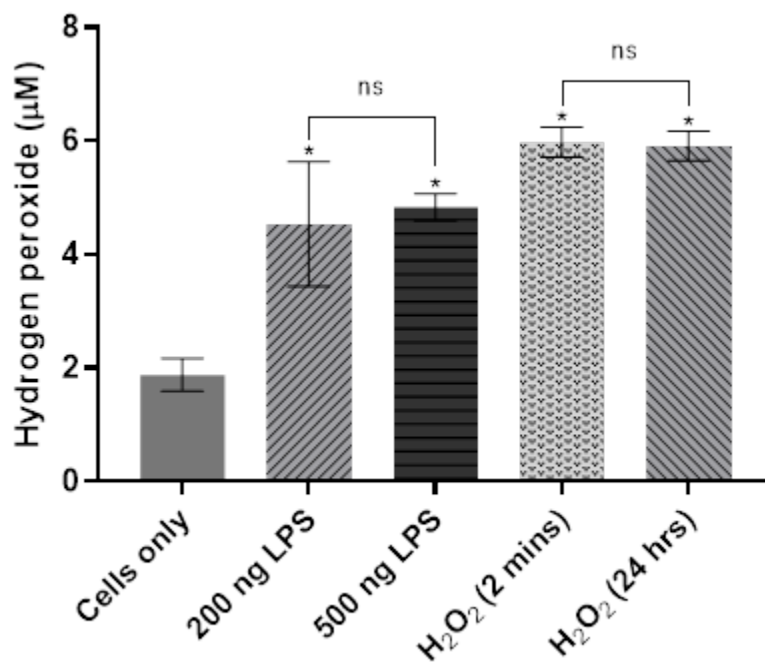


Figure 3-3: Effect of lipopolysaccharides (LPS) on hydrogen peroxide production in RAW 264.7 cells. Cells were seeded in 24-well cell culture plates at a density of 1×10^5 cells/well. Upon reaching 40-50% confluency, treated cells were spiked with LPS in two concentrations (200 ng/mL and 500 ng/mL, in triplicate), then incubated for 24 hours. After calibration of the Pt-MEA against H₂O₂ in complete cell culture medium (DMEM), amperometry was performed in each well for four minutes with a potential step of +0.7 V against an Ag/AgCl reference electrode. The sensitivity obtained during calibration (9.975 pA/µM; $R^2 = 0.9995$) was used to translate current for each experimental condition to normalized H₂O₂ concentration (µM). Data shown correspond to Electrode 1 (E1), the electrode nearest the cells. One-way ANOVA ($n = 5$, $p = 0.002$) was performed to assess the significance of differences among all group mean concentrations, followed by the Tukey-Kramer test to assess pairwise significant differences ($n = 5$, * $p < 0.05$, ** $p < 0.001$).

H₂O₂ showed apparent persistence in the 24-hour positive control: currents generated (i.e., H₂O₂ detected) at E1 in the H₂O₂ (2 mins) and H₂O₂ (24 hrs) groups were not significantly different ($p = 0.99998$). The normalized H₂O₂ concentration in both positive controls was ~6 µM—consistent with the expected ~4 µM increase above average H₂O₂ concentration in the cells-only negative control (1.88 ± 0.30 µM).

Given the possibility of macrophages metabolizing external H₂O₂ to concentrations below the LOD of the probe [50], the similar signals obtained in both

H₂O₂ positive controls indicate a robust ability to detect H₂O₂ incubated for long periods with live cells.

This result extended to LPS-doped cells as well (see above). Taken together, these two results validate the hypothesis that stable extracellular concentrations of LPS-induced H₂O₂ may be detected in RAW 264.7 cells via the probe.

3.2.3 Optimization of LPS Concentration

In order to find the optimal time, concentration, and pre-doping cell confluency for extracellular H₂O₂ production, two additional concentrations of LPS were included in the next experiment. RAW 264.7 cells were seeded in 24-well plates as above and doped with LPS in the following (final) concentrations: 200 ng/mL, 500 ng/mL, 800 ng/mL, and 1000 ng/mL. The cells were incubated for 12 or 24 hours before testing.

H₂O₂ production in RAW 264.7 cells showed no significant LPS dose dependence (Figure 3-4), implying that the range of LPS concentrations assayed, 200 ng/mL-1 µg/mL, is saturating yet sublethal.

Extracellular H₂O₂ production was more pronounced at the two lower concentrations of LPS (see Figure 3-4). Given the toxicity of LPS and the potential concomitant reduction in cell viability [51], the lowest dose, 200 ng/mL, was selected as the best concentration for further study.

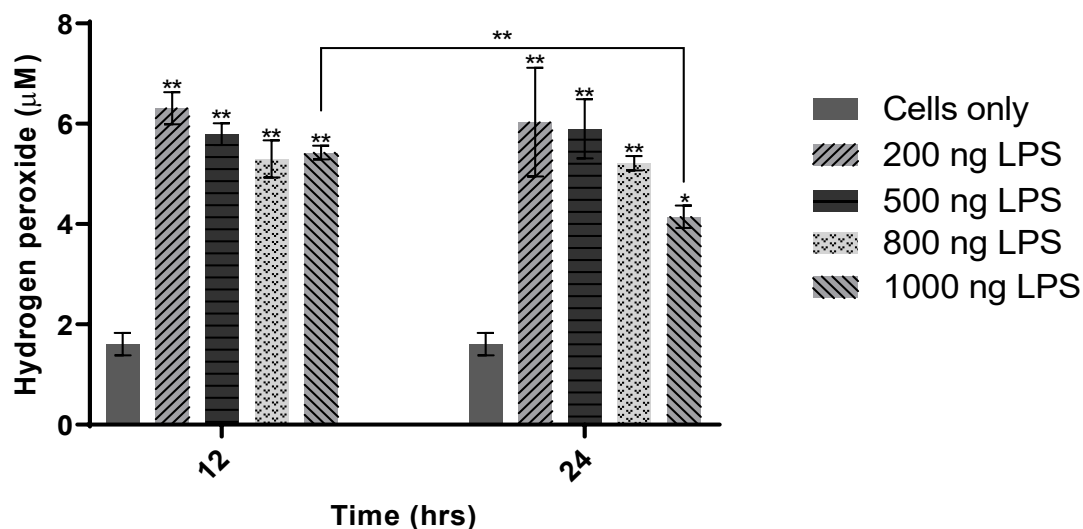


Figure 3-4: Effect of lipopolysaccharides (LPS) concentration on hydrogen peroxide production in RAW 264.7 cells. Four concentrations of H_2O_2 (200 ng/mL, 500 ng/mL, 800 ng/mL and 1000 ng/mL) were added to cells in triplicate. Cells were incubated 12 or 24 hours. The sensitivity obtained was $4.10 \text{ pA}/\mu\text{M}$ ($R^2 = 0.9995$). Data shown correspond to Electrode 1 (E1), the microelectrode nearest the cells. One-way ANOVA ($n = 14$, $p < 0.001$) and the Tukey-Kramer test ($n = 14$, $*p < 0.05$, $**p < 0.001$) were used to assess statistical significance.

The apparent stability of extracellular H_2O_2 was further supported by this experiment: between 12 hours and 24 hours, only the highest dosage of LPS ($1 \mu\text{g}/\text{mL}$) showed any statistically significant reduction in H_2O_2 detected by the probe (Figure 3-4).

3.2.4 Optimization of Incubation Time

Additional time studies were performed to discern the effect of incubation time on H_2O_2 production. The optimal LPS concentration of $200 \text{ ng}/\text{mL}$ was used. RAW 264.7 cells were seeded in 24-well plates as above, then doped with $200 \text{ ng}/\text{mL}$ LPS and incubated 6, 12, 24 or 48 hours (see Figure 3-5).

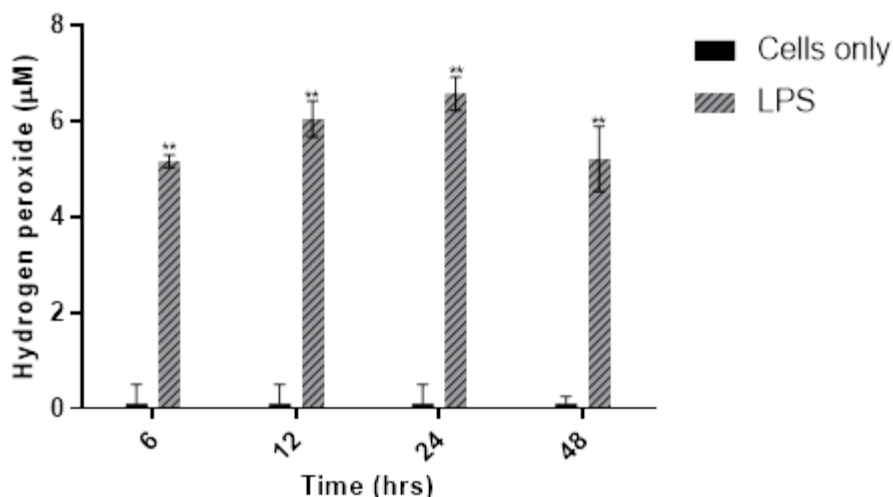


Figure 3-5: Effect of incubation time on hydrogen peroxide production in RAW 264.7 cells. 200 ng/mL LPS was added to cells plated in triplicate in 24-well plates (seeding density: 1×10^5 cells/mL). Cells were incubated 6, 12, 24 or 48 hours. Probe sensitivity: 11.0 pA/ μ M ($R^2 = 0.9997$). One-way ANOVA ($n = 21$, $p < 0.001$) and the Tukey-Kramer test ($n = 21$, $*p < 0.05$, $**p < 0.001$) were used to assess statistical significance.

At each of the four time points, H_2O_2 was significantly elevated in LPS-treated cells versus cell-only controls ($p < .001$). Somewhat unexpectedly, LPS-stimulated H_2O_2 detected was not statistically different across the four time points. This prolonged stability indicated that 200 ng/mL LPS produced a stable, saturating concentration of extracellular H_2O_2 . Selecting an optimal LPS incubation time was thus somewhat arbitrary; for convenience, 24 hours was chosen for future experiments.

3.2.5 Optimization of Incubation Temperature

The inflammatory response depends on metabolically functioning cells, which must initiate a host of synthetic and transport processes. Since the functioning of mammalian cells *in vitro* depends strongly on incubation temperature, it was expected that H_2O_2 production in LPS-doped RAW cells incubated at 4 °C would be near zero.

To assess the effect of reduced incubation temperature on H₂O₂ production, RAW 264.7 cells were seeded in 24-well plates as described above. All plates were initially incubated at 37 °C, 5% CO₂ to ensure the cells could adhere and proliferate. After we used Method 3 to dope the cells with 200 ng/mL LPS, one plate was removed to a 4 °C refrigerator. All plates were then incubated for 48 hours. Subsequent testing with the ROS probe revealed the expected lack of extracellular H₂O₂ produced by 4 °C-incubated cells (see Figure 3-6).

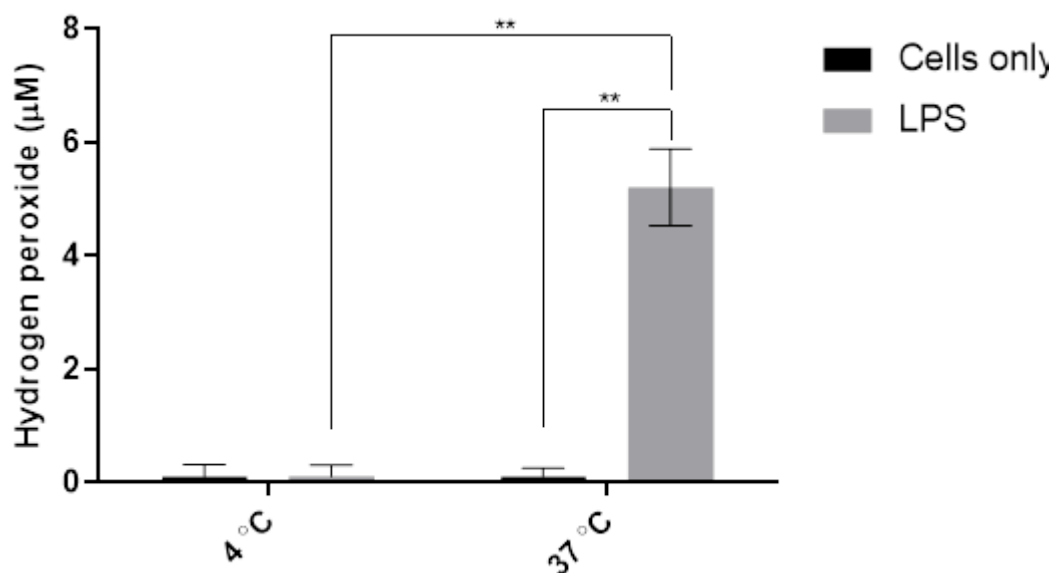


Figure 3-6: Effect of reduced incubation temperature on H₂O₂ production in RAW 264.7 cells. LPS-doped cells received 200 ng/mL in each well. Cells were incubated for 48 hours at 4 °C or 37 °C (5% CO₂) following addition of LPS. Probe sensitivity: 11.0 pA/µM; R², 0.9997. One-way ANOVA (n = 8, p < 0.001) and the Tukey-Kramer test (n = 14, *p < 0.05, **p < 0.001) were used to assess statistical significance.

3.2.6 Effect of Dexamethasone on H₂O₂ Production

The anti-inflammatory glucocorticoid drug dexamethasone (Dex) inhibits the production of pro-inflammatory cytokines (e.g., IL-6, IL-8, TNF-α), thereby reducing ROS/RNS production in M1 macrophages [55-56]. It was expected that Dex would

counter the action of LPS, thus reducing cumulative H_2O_2 production in LPS-doped RAW 264.7 cells [52]. To assess the effect of treating cells with Dex in conjunction with LPS, cells were treated with 200 ng/mL LPS and either 200 nM or 400 nM Dex, then incubated 6, 12, 24, or 48 hours (see Figure 3-7).

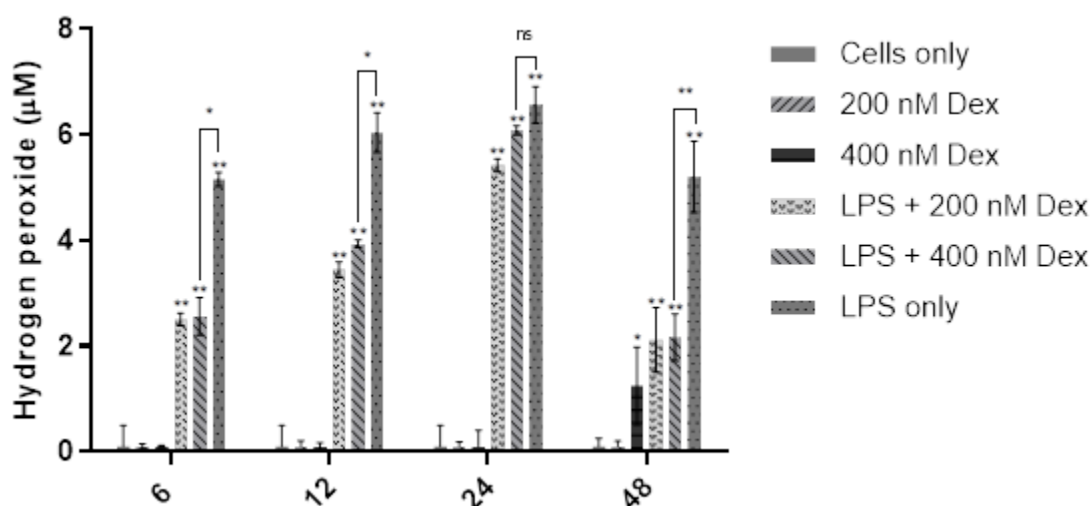


Figure 3-7: Effect of dexamethasone on H_2O_2 production in RAW 264.7 cells. Cells received 200 ng/mL LPS and/or 200 nM or 400 nM Dex in each well. Cells were incubated for 6, 12, 24, or 48 hours following addition of LPS and/or Dex. Probe sensitivity: 11.0 pA/ μM ; R^2 , 0.9997. One-way ANOVA ($n = 14$, $p < 0.001$) and the Tukey-Kramer test ($n = 14$, $*p < 0.05$, $**p < 0.001$) were used to assess statistical significance.

At each of the four time points, cells treated with LPS and Dex (200 nM and 400 nM) produced significantly more H_2O_2 than cell-only controls ($p < 0.001$). Thus, the pro-inflammatory effect of LPS was not completely abolished by either concentration of Dex. However, this effect was mitigated by Dex at three time points: at 6, 12, and 24 hours after treatment, LPS + Dex groups produced significantly less H_2O_2 than the LPS-only positive control (6 hours and 12 hours: $p < 0.05$; 24 hours: $p < 0.001$). Between 6 and 24 hours, these data appear to show the anti-inflammatory action of Dex being gradually outpaced by LPS-stimulated H_2O_2 production. Yet 48 hours after treatment, the anti-

inflammatory, ROS-suppressive effect was strongest ($p < 0.001$). Unexpectedly, Dex alone stimulated significant H_2O_2 production ($p < 0.05$) at 48 hours. This seeming paradox should be investigated further. Despite the imperfect trend in the data, these results support the hypothesis that the probe may be used as an extracellular assay not just of H_2O_2 , but of inflammation.

3.2.7 Effect of Cell Culture Plate Type on H_2O_2 Production

As a further optimization step, three types of cell culture plate—6-well, 12-well, and 24-well (with surface areas of, respectively, 9.6 cm^2 , 3.9 cm^2 , and 1.9 cm^2 per well) were seeded with RAW 264.7 cells and incubated/doped as above with 200 ng/mL or 500 ng/mL LPS (see Figure 3-8).

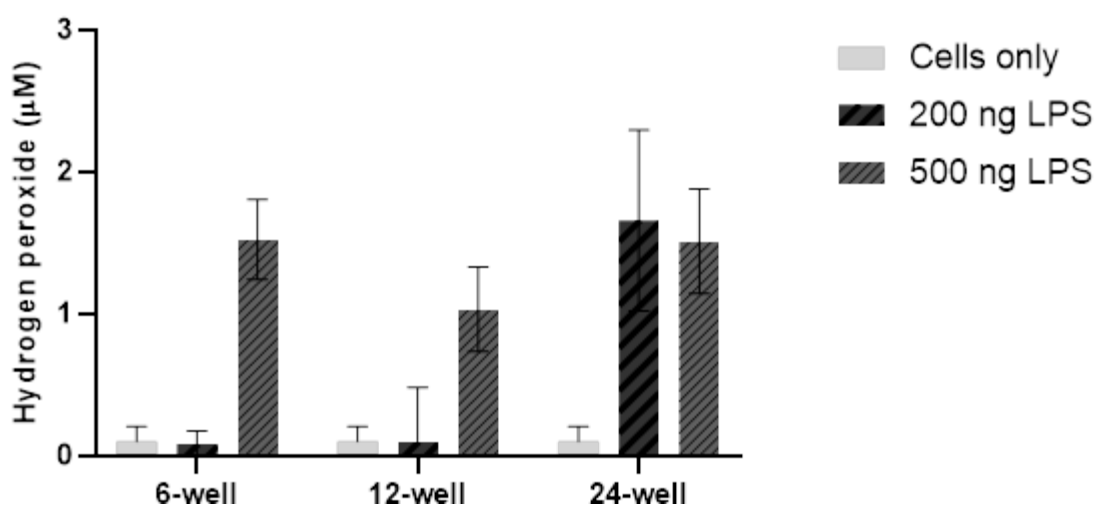


Figure 3-8: Effect of cell culture plate type on H_2O_2 production in RAW 264.7 cells. 6-well, 12-well, and 24-well plates were seeded with RAW 264.7 cells, grown to 40-50% confluency, and incubated with 200 ng/mL LPS for 24 hours. Probe sensitivity: $5.803 \text{ pA}/\mu\text{M}$; R^2 , 0.9985. One-way ANOVA ($n = 8$, $p < 0.001$) and the Tukey-Kramer test ($n = 14$, $*p < 0.05$, $**p < 0.001$) were used to assess statistical significance.

Because the 24-well plates led to greater cumulative H_2O_2 , they were selected for use in the remainder of the project.

The trend in the data was not clear enough to draw conclusions about, e.g., a relation among surface area of a given well, volume of media present, and H₂O₂ produced.

3.2.8 Viability Assay of LPS-Doped and ROS-Probed Cells

An MTT assay kit (Promokine) was used to assess viability of cells cultured in 96-well plates and subjected to one of the following conditions: 1) negative control, 2) 200 ng/mL LPS, 3) 500 ng/mL LPS, 4) exposure to the ROS probe (+0.7 V against Ag/AgCl) for 5 minutes, 5) exposure to the ROS probe (+0.3 V against Ag/AgCl) for 5 minutes.

At both 200 ng/mL and 500 ng/mL, RAW 264.7 cells exhibited viability slightly greater than 100% ($p > 0.05$): LPS appears to encourage proliferation at these doses (see Figure 3-9). This result agrees with a phenomenon observed in the inverted microscope: after incubation with LPS in 24-well plates, these cells often appeared more confluent than those of the negative control (data not shown).

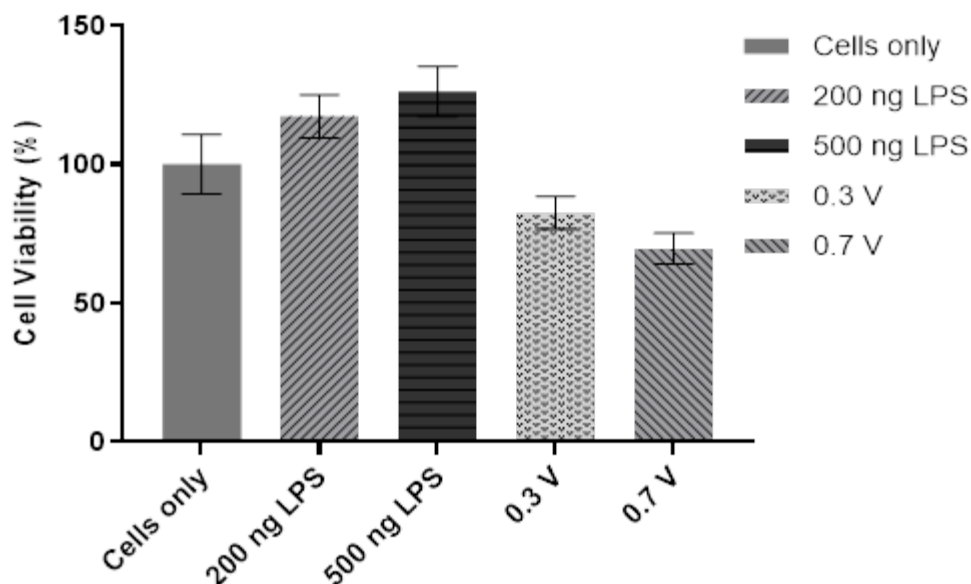


Figure 3-9: Effect of LPS or ROS probe operation on viability of RAW 264.7 cells. 96-well plates were seeded with 1×10^4 RAW 264.7 cells, grown to 50% confluency, and doped with 200 ng/mL or 500 ng/mL LPS, or probed at one of two potential steps: +0.7 V and +0.3 V. One-way ANOVA ($n = 6$, $p = 0.0029$) and Tukey-Kramer post-hoc analysis ($n = 6$, $*p < 0.05$, $**p < 0.001$) were performed.

Tukey-Kramer analysis of these results indicated that neither LPS doping nor use of the probe significantly reduced cell viability ($p > 0.05$). At both 200 ng/mL and 500 ng/mL, RAW 264.7 cells exhibited viability slightly greater than 100% ($p > .05$): LPS appears to be mildly pro-proliferative at these doses. This result agrees with a phenomenon observed in the inverted microscope: after incubation with LPS in 24-well plates, these cells often appeared more confluent than those of the cell-only control. This effect raises the question: might the greater number of cells account for some of the increase in cumulative H_2O_2 seen in LPS-doped groups?

The reduction in viability at both voltage steps was just shy of statistical significance. However, in this assay the probe was used in 100 μ L, rather than 1 mL, of media (i.e., a 96-well plate, rather than a 24-well plate). It is possible that the closer

confines of the 96-well plate caused additional stress to the cells when the probe was introduced and operated.

3.2.9 Optimization of the Calibration Protocol

At the outset of this project, fresh media warmed to 37 °C in a water bath (VWR) was used to calibrate the probe. However, the E1 baseline current obtained was often notably larger than the analogous current in cell-containing media—implying a large, negative concentration of H₂O₂ in the cells.

While consumption of extracellular H₂O₂ by RAW 264.7 cells is demonstrated in the literature, as is photochemical production of H₂O₂ in cell culture media by exposure to light, the elucidation of these mechanisms is beyond the scope of this thesis [53-54].

To ensure a calibration medium more electrochemically similar to the cell-only control, the calibration protocol was modified to incorporate spent, cell-containing media: a separate, 24-well plate containing only cells and media was included in each experiment. Prior to calibration, 10 mL of spent media was aspirated from this 24-well plate and added to a 20-mL beaker. Calibration was then performed as above. The E1 baseline currents obtained from this modified protocol were consistently closer to those of the cell-only control (data not shown).

CHAPTER 4

CONCLUSIONS AND FUTURE DIRECTIONS

This work provides a robust demonstration of a novel use of Pt MEA probes. Stable concentrations of extracellular H₂O₂ released *in vitro* by macrophages placed under oxidative stress were detected up to 48 hours after doping with LPS. The Pt MEA was used to quickly and quantitatively measure the anti-inflammatory effect of dexamethasone on LPS-doped RAW 264.7 cells. This experiment served as an *in vitro* model of an inflammatory assay.

Future work with this probe will involve the multiplexing of this assay to allow for additional ROS/RNS sensing (e.g., the simultaneous detection of H₂O₂ and nitric oxide with separate microelectrodes). Further modifications of the Pt MEA will allow such multiplexed sensing in conjunction with the monitoring of treatment (e.g., the depletion of therapeutic antioxidants such as ascorbic acid). This additional work would point toward the creation of a convenient, comprehensive clinical assay of oxidative stress and inflammation.

APPENDIX A
MATLAB SCRIPT FOR DATA ANALYSIS


```

% Data-analysis program for ROS Project
% Written by: Victor Carriere
% 4/29/19
%
% This program imports FAST system data (Excel only) and averages current
% at a user-specified number of time points (usually across the last minute of
% testing) to extract one current value, in pA, for each trial. The user
% also selects and names experimental groups and enters calibration
% equations for each electrode (E1 and E2 only, in practice). One-way ANOVA and the
% Tukey-Kramer test are performed on the user-selected groups. Results of the assay are
% exported to the table "resultstab" in the workspace and to an Excel file %that the user
% names. Results included in the Excel sheet:
%
%
% 1. Mean raw current + SEM (pA)
% 2. Mean normalized current + SEM (pA)
% 3. Mean normalized concentration + SEM ( $\mu\text{M}$ )
% 4. Results of the statistical analysis (see above)

```

```

%Storing prompts to be used in the dialog box below:
filenameprompt = 'Input name of results spreadsheet';
grpprompt = 'Input number of experimental groups (e.g., for an experiment...with only two
concentrations of LPS and one control, input 3)';
freqprompt = 'Enter number of measurements per second (see analysis folder for frequency
in Hz)';
totalptsprompt = 'Enter number of time points to include (default: 50)';
startprompt = 'Enter initial time of analysis in seconds (default: 180)';
finishprompt = 'Enter final time of analysis in seconds (default: 240)';

```

```

%The dialog box
speccell = inputdlg({filenameprompt,grpprompt, freqprompt, totalptsprompt, startprompt,
finishprompt});
tabfile = speccell{1};

```

```

%Converts user entries from 1. a cell array of character vectors (~strings) -> 2. matrix
of
%numbers (doubles) -> 3. cell array with each user entry stored as a number
%in a single cell. Cells are easily split and assigned to different
%variables (see line 37).
speccellnum = num2cell(str2double(speccell(2:end)));
%speccell(1)=[]; %deletes first row, leaving only numeric user entries
%Assigns variable names to user entries
[grps, freq, totalpts, start, finish] = speccellnum{:}; %assigns user entries to
variables

```

```

%defines cell array with dimensions 2 x (number of groups), for storing
%filenames and paths
fullpaths = cell(2,grps);

```

```

%Prompts users to select files for each group; group names are stored in
%{1,n} of the the cell array "fullpaths"; a variable number of spreadsheets is
%imported and stored in {2,n} as a cell array.
for n = 1:grps
    groupprompt = (['Input name of Group ' num2str(n)]);
    grpassign = inputdlg(groupprompt);
    fullpaths{1,n} = grpassign;
    fileprompt = (['Select files in Group ' num2str(n)]);

    [filename,filepath] = uigetfile('*.xlsx;*.xls',...
        fileprompt, 'C:\Users\Victor\Desktop\Organized ROS data 6.20.19\Raw
Data','MultiSelect', 'on');
    %Organized ROS Data 6.20.19',...
    % 'MultiSelect', 'on');

%end

%For each experimental group named in {1,n}, creates a cell in {2,n}...
%with each complete filename in the group as an element of that cell. A
%10-trial Group 3 would have 10 filenames stores in one cell in fullpaths (cell {2,3}).
fullpaths{2,n} = fullfile(filepath,filename);

%Begins terminating script if user cancels file choosing
if isequal(filename, 0)
    disp('User canceled file choosing');
    return;

else
    %disp([fullpaths{1,n} ':' fullpaths{2,n}]);

end
end

%preallocating memory for cell array of imported spreadsheets
spreads = cell(2, grps); %2 rows x the number of groups
spreads(1,:) = fullpaths(1,:); %copies the full filenames/paths from fullpaths to the
first row of spreads

%For each group, imports the spreadsheet data corresponding to
%the selected files and stores in {2,n} for Group n
for n=1:grps

    %Importing the lone spreadsheet for the one-file case in a given group (the
    %path name is stored as a character vector for one file, but as a cell
    %array containing multiple character vectors for more than one file).
    tf = isa(fullpaths{2,n}, 'char');

        if tf==1

            %Even though fullpaths{2,n} already contains the complete filename as a
            %character vector, xlsread interprets xlsread(fullfile(fullpaths{2,n})) as
            %applying to the first letter of the file path, i.e., "C" for
            %many hard drives.
            %char(fullfile(fullpaths{2,n})) renders the filename legible to xlsread.

```

```

        spreads{2,n} = {xlsread(char(fullpaths{2,n}))};

    else

        for ii=1: numel(fullpaths{2,n})
            spreads{2,n}{1,ii}=xlsread(char(fullpaths{2,n}{1,ii})); %all groups
with >1 file imported here
        end
    end
end

%concatenates all spreadsheets into a one-row cell array
spreadscat = [spreads{2,:}]; %I don't know why spreads exists then. Can go directly to
spreadscat it seems.

%Dialog box prompts user for slope and intercept of each linear-fit line
%from calibration curves.
precal = inputdlg({'E1 - precal slope','E1 - precal intercept','E2 - precal slope'...
    'E2 - precal intercept', 'E3 - precal slope', 'E3 - precal
intercept'...
    'E4 - precal slope', 'E4 - precal intercept'},...
    'Precalibration(y = mx + b)', [1 50; 1 50;...
    1 50; 1 50; 1 50; 1 50; 1 50; 1 50]); %length specifications for
input fields

precaldub = str2double(precal); %Converts user-entered values from strings to numeric
data in a cell array
precaldub = reshape(precal,2,[]); %reshapes to a 2-row cell with slopes in row 1,
intercepts in row 2
precal slopes = precaldub(1,:); %slopes reassigned to this one-row cell array
rprecal slopes = str2double(repmat(precal slopes,size(spreadscat,2),1)); %vertically stacks
precal slopes n times for n trials
precalints = precaldub(2,:); %intercepts here
rprecalints = str2double(repmat(precalints,size(spreadscat,2),1));

%The same, but for the post-test calibration
postcal = inputdlg({'E1 - postcal slope','E1 - postcal intercept','E2 - postcal slope'...
    'E2 - postcal intercept', 'E3 - postcal slope', 'E3 - postcal
intercept'...
    'E4 - postcal slope', 'E4 - postcal intercept'},...
    'postcalibration(y = mx + b)', [1 50; 1 50;...
    1 50; 1 50; 1 50; 1 50; 1 50; 1 50]);
postcaldub = str2double(postcal); %Converts user-entered data (strings) to numeric data
postcaldub = reshape(postcal,2,[]); %reshapes to a 2-row matrix with slopes in row 1,
intercepts in row 2
postcal slopes = postcaldub(1,:); %slopes reassigned to this matrix
rpostcal slopes = str2double(repmat(postcal slopes,size(spreadscat,2),1));
postcalints = postcaldub(2,:); %intercepts here
rpostcalints = str2double(repmat(postcalints,size(spreadscat,2),1));

avgints=mean(cat(3,rpreints,rpostints),3); %gives media baselines corresponding to which
will be used to normalize current only.

```

```

%stores number of elements in each group in order of selection
groupsizes = cellfun('length', spreads(2,:));

%These function calls complete the analysis. They export a table to Excel, then read the
spreadsheet
%back into Matlab as the table "resultstab" for convenience (double-click resultstab in
the workspace to see the table).
%On PC, the Excel sheet will be in the MATLAB directory in...
%Documents by default. The code for the functions is below.
[rawscollct,rownums] = currents(spreadscat, freq, totalpts, start, finish, spreads);
%Extracting linearly spaced time points (row numbers) from each trial for analysis
avgpAcollect = averagecurr(rawscollct); %calculates un-normalized current; needed for
finding concentration
[avgcurrent,preconc,postconc] =
regroup1(avgpAcollect,rpreslopes,rpreints,rpostslopes,rpostints); %calculates precal and
postcal concentration
[allresults,allmeans,allvalsprereshape,allsems,cellvals] =
fix(avgcurrent,preconc,postconc,groupsizes,grps);
normalpasprecalonly = avgcurrent - avgints; %normalizes current to precal media baseline
normalvals=givenorm(normalpasprecalonly,groupsizes,grps); %calculates
resultstab = tableout(fullpaths,allresults,grps,tabfile,normalvals);
[repcol,resultstab2] =
rep(tabfile,fullpaths,grps,groupsizes,avgcurrent,preconc,postconc,normalpasprecalonly);
statstab2=statsout(fullpaths,grps,preconc,normalpasprecalonly,repcol,tabfile);
%*****

%Extracts current data from each desired time point, for each of the four
%electrodes. Returns a cell array with an n x 4 array of currents
%(converted from nA to pA) corresponding to each individual replicate.
function [rawspA, rownums] = currents(x, freq, totalpts, start, finish, spreads)
%rawspA = cell(size(x));
rawspA = cell(size(x));
totalptsmat=(0:(totalpts-1));
nvals=1:4;
%If testing for any replicate was stopped a few seconds early, the finish
%time (typically 4 or 8 minutes) is adjusted and evenly spaced time points
%selected for each replicate between, e.g. 3:00 and 3:58 instead of 3:00
%and 4:00:
testcat=horzcat(spreads{2,:}); %replace with spreadscat (already exists)!
for ii = 1:numel(testcat)
    rowsmat(ii) = size(testcat{ii},1);
end

if min(rowsmat) < (freq*finish+1)
    rownums = round(linspace(freq*start+1,min(rowsmat),totalpts));
else
    rownums = round(linspace(freq*start+1,freq*finish+1,totalpts));
end

```

```

for n=1:numel(x)
rawsnA = x{1,n}(rownums, 2*nvals);
rawspA{1,n} = 1000.*((-1).*(rawsnA)-1.4);
end

end

%Finds average current (pA) across extracted data; each column in currpAallpts
corresponds
%to one of four electrodes in a given trial. Hence currpAallpts contains
%(# of time points)(4 electrodes)(total # of trials selected) elements.
function avgcurrpA = averagecurr(x)

currpAallpts = cell2mat(x);
%avgpAvals = zeros(1,spreadcatcols);
avgcurrpA = mean(currpAallpts);
end

%Groups all average-current data (for all groups and trials) by electrode: column 1
corresponds
%to electrode 1 (E1), column 2 to electrode 2 (E2)...
function [fourcols, prevals, postvals] = regroup1(x, rpreslopes,
rpreints,rpostslopes,rpostints)

fourcols = reshape(x,4,[]).'; %columns: E1 E2 E3 E4 in pAv

%Vertically stacks slope and intercept row matrices: n trials -> n rows.
%Converts values to concentration:  $x = (y - b)/m$ 
%(columns: E1 E2 E3 E4 in  $\mu\text{M}$ )
prevals = (fourcols - rpreints)./(rpreslopes);
postvals = (fourcols - rpostints)./(rpostslopes);
%fourcols(:,1,2) = (fourcols - precal(2))/(precal(1)) %convert to concentration in  $\mu\text{M}$ 
based on precalibration curve
%fourcols(:,:,3) = (fourcols - postcal(2))/(postcal(1))
end

function [allresults, allmeans,allvals, allsems,cellvals] =
fix(x,prevals,postvals,groupsizes,grps)

allvals = horzcat(x, prevals,postvals); %horizontally concatenates results matrices (12
columns): Current E1-E4 (all trials), Precal E1-E4 (all trials), Postcal E1-E4 (all
trials)
cellvals = mat2cell(allvals, groupsizes,12); %Converts the 12-column results matrix into
a cell array divided sequentially by the number of elements per group: if group 1 had 4
trials and group 2 had 3, then cell {1,1} of cellvals consists of a 4x12 matrix, cell
{2,2} of a 3x12 matrix, etc.
for ii=1:grps
if size(cellvals{ii,1},1)==1
allmeans(ii,1)=cellvals(ii,1);
allsems(ii,1) = {zeros(1,12)};
else
allmeans(ii,1) = cellfun(@mean, cellvals(ii,1),'UniformOutput',false); % Cellfun
applies mean and SEM to each column
allsems(ii,1) = cellfun(@sem, cellvals(ii,1),'UniformOutput',false); %

```

```

end
end
allresults(1:grps,1:2:23)=cell2mat(allmeans);
allresults(1:grps,2:2:24)=cell2mat(allsems);

function givesem = sem(x)
givesem = std(x)./sqrt((size(x,1)));
end

end

function normalcurrent = givenorm(normalpas,groupsizes,grps)
normalcellvals = mat2cell(normalpas, groupsizes,4);
for ii=1:grps
    if size(normalcellvals{ii,1},1)==1
        normmeans(ii,1)=normalcellvals(ii,1);
        normsems(ii,1) = {zeros(1,4)};
    else
        normmeans(ii,1) = cellfun(@mean, normalcellvals(ii,1),'UniformOutput',false); %
        Cellfun applies mean and SEM to each cell in the array; cells are now divided by group
        normsems(ii,1) = cellfun(@sem, normalcellvals(ii,1),'UniformOutput',false); %
    end
end
end
normalcurrent(1:grps,1:2:7)=cell2mat(normmeans);
normalcurrent(1:grps,2:2:8)=cell2mat(normsems);

function givesem = sem(x)
givesem = std(x)./sqrt((size(x,1)));
end
end

function givetable = tableout(fullpaths,allresults,grps,tabfile,normalvals)

currentrowheadings =
{'E1_avg_current', 'SEM_E1_current', 'E2_avg_current', 'SEM_E2_current', ...
    'E3_avg_current', 'SEM_E3_current', 'E4_avg_current', 'SEM_E4_current'};

precalrowheadings = {'E1_precal_conc', 'SEM_E1_precal', 'E2_precal_conc', ...
    'SEM_E2_precal', 'E3_precal_conc', 'SEM_E3_precal', 'E4_precal_conc', ...
    'SEM_E4_precal'};

postcalrowheadings = {'E1_postcal_conc', 'SEM_E1_postcal', 'E2_postcal_conc',
    'SEM_E2_postcal_cont', ...
    'E3_postcal_conc', 'SEM_E3_postcal', 'E4_postcal_conc', 'SEM_E4_postcal'};

normrowheadings =
{'E1_norm_current', 'SEM_E1_norm_current', 'E2_norm_current', 'SEM_E2_norm_current', ...
    'E3_norm_current', 'SEM_E3_norm_current', 'E4_norm_current',
    'SEM_E4_norm_current'};

grpcols = string(fullpaths(1,:)); %vertical column of sample IDs (MC2, MC4...)

```

```

coltable = table(grpcols,'VariableNames',{'Sample_ID'}); %creates one-column "table" from
grpcols to be appended to results tables below
currstring = cellstr(currentrowheadings);
precalstring = cellstr(precalrowheadings);
postcalstring = cellstr(postcalrowheadings); %converts above headings to cell arrays of
character vectors (cannot be incorporated into tables otherwise)
normcurrstring = cellstr(normrowheadings);
%allresults = num2cell(allresults); %

currtable = array2table(allresults(:,1:8),'VariableNames',currstring);
currtable = [coltable currtable];
precaltable = array2table(allresults(:,9:16),'VariableNames',precalstring);
precaltable = [coltable precaltable];
postcaltable = array2table(allresults(:,17:24),'VariableNames',postcalstring);
postcaltable = [coltable postcaltable];
normcurrtable = array2table(normalvals,'VariableNames',normcurrstring);
normcurrtable = [coltable normcurrtable];

currcellrange = ['A',num2str(3),':','I',num2str(grps+3)];
precalcellrange = ['A',num2str(grps+7),':','I',num2str(2*grps+7)];
postcalcellrange = ['A',num2str(2*grps+11),':','I',num2str(3*grps+11)];
normcurrcellrange = ['A',num2str(3*grps+15),':','I',num2str(4*grps+15)];

writetable(currtable, [tabfile,'.xlsx'], 'Range',currcellrange);
writetable(precaltable, [tabfile,'.xlsx'], 'Range',precalcellrange);
writetable(postcaltable, [tabfile,'.xlsx'], 'Range',postcalcellrange);
writetable(normcurrtable, [tabfile,'.xlsx'], 'Range',normcurrcellrange);

givetable = readtable([tabfile,'.xlsx']);
end

function [repcol,reptabletest] =
rep(tabfile,fullpaths,grps,groupsizes,avgcurrent,preconc,postconc,normalpasprecalonly)
grpsum = sum(groupsizes);
repcol = repelem(fullpaths(1,:),groupsizes)';
currentrepheadings = {'E1_avg_current','E2_avg_current','E3_avg_current',
'E4_avg_current'};
currrepstr = cellstr(currentrepheadings);
precalrepheadings =
{'E1_precal_conc','E2_precal_conc','E3_precal_conc','E4_precal_conc'};
precalrepstr = cellstr(precalrepheadings);
postcalrepheadings =
{'E1_postcal_conc','E2_postcal_conc','E3_postcal_conc','E4_postcal_conc'};
postcalrepstr = cellstr(postcalrepheadings);
normrepheadings =
{'E1_norm_current','E2_norm_current','E3_norm_current','E4_norm_current'};
normrepstr = cellstr(normrepheadings);

%repcoltable = table(testrep2);
repcoltable = table(repcol,'VariableNames',{'Group'});
rawcurrtable = array2table(avgcurrent,'VariableNames',currrepstr);
rawcurrtable = [repcoltable rawcurrtable];
precalreptable = array2table(preconc,'VariableNames',precalrepstr);
precalreptable = [repcoltable precalreptable];

```

```

postcalreptable = array2table(postconc, 'VariableNames', postcalrepstr);
postcalreptable = [repcoltable postcalreptable];
normreptable = array2table(normalpasprecalonly, 'VariableNames', normrepstr);
normreptable = [repcoltable normreptable];
reptabletest = normreptable;

startingrow = 4*grps+18;
currreprange = ['A', num2str(startingrow), ':', 'E', num2str(startingrow+grpsum)];
precalreprange =
['A', num2str(startingrow+grpsum+4), ':', 'E', num2str(startingrow+2*grpsum+4)];
postcalreprange =
['A', num2str(startingrow+2*grpsum+8), ':', 'E', num2str(startingrow+3*grpsum+8)];
normcurrreprange =
['A', num2str(startingrow+3*grpsum+12), ':', 'E', num2str(startingrow+4*grpsum+12)];

writetable(rawcurrtable, [tabfile, '.xlsx'], 'Range', currreprange);
writetable(precalreptable, [tabfile, '.xlsx'], 'Range', precalreprange);
writetable(postcalreptable, [tabfile, '.xlsx'], 'Range', postcalreprange);
writetable(normreptable, [tabfile, '.xlsx'], 'Range', normcurrreprange);

givetable = readtable([tabfile, '.xlsx']);

end

function statstab2 = statsout(fullpaths, grps, precon, normalpasprecalonly, repcol, tabfile)
[~, e1preconctab, e1preconstats] = anova1(precon(:, 1), string(repcol));
[~, e1normcurrtab, e1normcurrstats] = anova1(normalpasprecalonly(:, 1), string(repcol));

e1preconctab2 = array2table(e1preconctab);
e1normcurrtab2 = array2table(e1normcurrtab);

[preconmultcomp, ~, ~, ~] = multcompare(e1preconstats);
[normcurrmultcomp, ~, ~, ~] = multcompare(e1normcurrstats);
preconmulttab = array2table(preconmultcomp);
normmulttab = array2table(normcurrmultcomp);

Group_names(1, 1:grps) = fullpaths(1, :);
Group_names2 = array2table(Group_names);
writetable(Group_names2, [tabfile, '.xlsx'], 'Sheet', 2, 'Range', 'A1');
writetable(Group_names2, [tabfile, '.xlsx'], 'Sheet', 3, 'Range', 'A1');
writetable(Group_names2, [tabfile, '.xlsx'], 'Sheet', 4, 'Range', 'A1');
writetable(Group_names2, [tabfile, '.xlsx'], 'Sheet', 5, 'Range', 'A1');

```



```
writetable(e1preconctab2, [tabfile, '.xlsx'], 'Sheet', 2, 'Range', 'A5');  
writetable(preconcmulttab, [tabfile, '.xlsx'], 'Sheet', 3, 'Range', 'A5');  
writetable(e1normcurrtab2, [tabfile, '.xlsx'], 'Sheet', 4, 'Range', 'A5');  
writetable(normmulttab, [tabfile, '.xlsx'], 'Sheet', 5, 'Range', 'A5');  
  
statstab2 = tabfile;  
  
end
```

Published with MATLAB® R2019a

BIBLIOGRAPHY

- [1] K. Krumova and G. Cosa, “Chapter I: Overview of reactive oxygen species,” in *Singlet Oxygen : Applications in Biosciences and Nanosciences, Volume 1*, 2016, p. 21.
- [2] H. Sies, C. Berndt, and D. P. Jones, “Oxidative stress,” *Annu. Rev. Biochem.*, vol. 86, pp. 715–748, 2017.
- [3] B. Kalyanaraman, “Teaching the basics of redox biology to medical and graduate students: Oxidants, antioxidants and disease mechanisms,” *Redox Biol.*, vol. 1, no. 1, pp. 244–257, 2013.
- [4] M.-Y. Liou and P. Storz, “Reactive oxygen species in cancer,” *Free Radic Res.*, vol. 44, no. 5, 2010.
- [5] H. Tan, N. Wang, S. Li, M. Hong, X. Wang, and Y. Feng, “The reactive oxygen species in macrophage polarization: reflecting its dual role in progression and treatment of human diseases,” *Oxid. Med. Cell. Longev.*, vol. 2016, p. 16 pages, 2016.
- [6] R. Medzhitov, “Origin and physiological roles of inflammation,” *Nature*, vol. 454, no. 7203. Nature Publishing Group, pp. 428–435, 24-Jul-2008.
- [7] C. Wittmann, P. Chockley, S. K. Singh, L. Pase, G. J. Lieschke, and C. Grabher, “Hydrogen peroxide in inflammation: messenger, guide, and assassin,” *Adv. Hematol.*, vol. 2012, pp. 1–6, Jun. 2012.
- [8] D. B. Hibbert, *Introduction to Electrochemistry*. London: Macmillan Press, 1993.
- [9] H. H. Girault, *Analytical and Physical Electrochemistry*. New York: EPFL Press, 2004.
- [10] H. Sies, “Role of metabolic H₂O₂ generation,” *J. Biol. Chem.*, vol. 289, no. 13, pp. 8735–8741, 2014.

- [11] J. F. Turrens, "Superoxide production by the mitochondrial respiratory chain," *Biosci. Rep.*, vol. 17, no. 1, pp. 3–8, 1997.
- [12] J. A. Imlay, "Cellular defenses against superoxide and hydrogen peroxide," *Annu. Rev. Biochem.*, no. September, pp. 755–776, 2008.
- [13] D. T. Antoine Carlioz, "Isolation of superoxide dismutase mutants in *Escherichia coli*: is superoxide dismutase necessary for aerobic life?," *EMBO J.*, vol. 5, no. 3, pp. 623–630, 1986.
- [14] M. J. Davies, "Protein oxidation and peroxidation," *Biochem. J.*, vol. 473, pp. 805–825, 2016.
- [15] J. E. Hall, *Guyton and Hall Textbook of Medical Physiology*. Philadelphia: Elsevier, 2016.
- [16] U. Förstermann and W. C. Sessa, "Nitric oxide synthases: regulation and function," *Eur. Heart J.*, vol. 33, pp. 829–837, 2012.
- [17] D. G. H. Sergey I. Dikalov, "Methods for detection of mitochondrial and cellular reactive oxygen species," *Antioxidants Redox Signal.*, vol. 20, no. 2, pp. 372–382, 2014.
- [18] P. Pacher, J. S. Beckman, and L. Liaudet, "Nitric oxide and peroxynitrite in health and disease," *Physiol. Rev.*, vol. 87, no. 1, pp. 315–424, 2007.
- [19] C. C. Winterbourn, "The biological chemistry of hydrogen peroxide," in *Methods in Enzymology*, vol. 528, Academic Press Inc., 2013, pp. 3–25.
- [20] C. C. Winterbourn, "Reconciling the chemistry and biology of reactive oxygen species," *Nat. Chem. Biol.*, vol. 4, no. 5, pp. 278–286, 2008.
- [21] H. Sies, "Hydrogen peroxide as a central redox signaling molecule in physiological oxidative stress: Oxidative eustress," *Redox Biol.*, vol. 11, pp. 613–619, 2017.
- [22] K. M. Holmström and T. Finkel, "Cellular mechanisms and physiological consequences of redox-dependent signalling," *Nat. Rev. Mol. Cell Biol.*, vol. 15, no. 6, pp. 411–421, 2014.
- [23] M. Rath, I. Müller, P. Kropf, E. I. Closs, and M. Munder, "Metabolism via arginase or nitric oxide synthase: two competing arginine pathways in macrophages," *Front. Immunol.*, vol. 5, no. 532, 2014.
- [24] A. Sica and A. Mantovani, "Macrophage plasticity and polarization: in vivo veritas," *J. Clin. Invest.*, vol. 122, no. 3, 2012.

- [25] F. C. Fang, “Antimicrobial actions of reactive oxygen species,” *mBio*, vol. 2, no. 5, 2011.
- [26] C. C. Winterbourn, A. J. Kettle, and M. B. Hampton, “Reactive oxygen species and neutrophil function,” *Annu. Rev. Biochem.*, vol. 85, no. 1, pp. 765–792, 2016.
- [27] W. M. Nauseef, “The phagocyte NOX2 NADPH oxidase in microbial killing and cell signaling,” *Curr. Opin. Immunol.*, vol. 60, pp. 130–140, 2019.
- [28] V. Ponath and B. Kaina, “Death of monocytes through oxidative burst of macrophages and neutrophils: Killing in Trans,” *PLoS One*, vol. 12, no. 1, pp. 1–20, 2017.
- [29] B. Taciak *et al.*, “Evaluation of phenotypic and functional stability of RAW 264.7 cell line through serial passages,” *PLoS One*, vol. 13, no. 6, pp. 1–13, 2018.
- [30] W. C. Raschke, S. Baird, P. Ralph, and I. Nakoinz, “Functional macrophage cell lines transformed by Abelson Leukemia Virus,” *Cell*, vol. 15, no. September, pp. 261–267, 1978.
- [31] S. Varma and B. Mattiasson, “Amperometric biosensor for the detection of hydrogen peroxide using catalase modified electrodes in polyacrylamide,” *J. Biotechnol.*, vol. 119, no. 2, pp. 172–180, 2005.
- [32] M. Ksibi, “Chemical oxidation with hydrogen peroxide for domestic wastewater treatment,” *Chem. Eng. J.*, vol. 119, no. 2–3, pp. 161–165, Jun. 2006.
- [33] C. Amatore, S. Arbault, Y. Chen, C. Crozatier, and I. Tapsoba, “Electrochemical detection in a microfluidic device of oxidative stress generated by macrophage cells,” *Lab Chip*, vol. 7, no. 2, pp. 233–238, 2007.
- [34] B. Kalyanaraman *et al.*, “Measuring reactive oxygen and nitrogen species with fluorescent probes: challenges and limitations.,” *Free Radic. Biol. Med.*, vol. 52, no. 1, pp. 1–6, 2012.
- [35] J. F. Woolley, J. Stanicka, and T. G. Cotter, “Recent advances in reactive oxygen species measurement in biological systems,” *Trends Biochem. Sci.*, vol. 38, no. 11, pp. 556–565, 2013.
- [36] I. Hossain *et al.*, “A novel microbiosensor microarray for continuous ex vivo monitoring of gamma-aminobutyric acid in real-time,” *Front. Neurosci.*, vol. 12, no. August, pp. 1–13, 2018.
- [37] J. L. Scoggin *et al.*, “An enzyme-based electrochemical biosensor probe with sensitivity to detect astrocytic versus glioma uptake of glutamate in real time in vitro,” *Biosens. Bioelectron.*, vol. 126, pp. 751–757, Feb. 2019.

- [38] S. Mateen, S. Moin, A. Qayyum Khan, A. Zafar, and N. Fatima, "Increased reactive oxygen species formation and oxidative stress in rheumatoid arthritis," *PLoS One*, vol. 11, no. 4, p. e0152925, 2016.
- [39] D. Aletaha and J. S. Smolen, "Diagnosis and management of rheumatoid arthritis: a review," *JAMA - J. Am. Med. Assoc.*, vol. 320, no. 13, pp. 1360–1372, 2018.
- [40] Carol A Hitchon and Hani S El-Gabalawy, "Oxidation in rheumatoid arthritis," *Arthritis Res. Ther.*, vol. 6, pp. 265–278, 2004.
- [41] E. Ho, K. Karimi Galoughi, C. C. Liu, R. Bhindi, and G. A. Figtree, "Biological markers of oxidative stress: Applications to cardiovascular research and practice," *Redox Biol.*, vol. 1, no. 1, pp. 483–491, 2013.
- [42] I. Tabas and K. E. Bornfeldt, "Macrophage phenotype and function in different stages of atherosclerosis hhs public access," *Circ. Res.*, vol. 118, no. 4, pp. 653–667, 2016.
- [43] M. Naghavi *et al.*, "From vulnerable plaque to vulnerable patient," *Circulation*, vol. 108, no. 14, pp. 1664–1672, 2003.
- [44] A. J. Kattoor, N. V. K. Pothineni, D. Palagiri, and J. L. Mehta, "Oxidative stress in atherosclerosis," *Curr. Atheroscler. Rep.*, vol. 19, no. 11, 2017.
- [45] D. R. Brenner *et al.*, "A review of the application of inflammatory biomarkers in epidemiologic cancer research," *Cancer Epidemiol Biomarkers Prev*, vol. 23, no. 9, 2014.
- [46] C. Aldridge, A. Razzak, T. A. Babcock, W. S. Helton, and N. J. Espat, "Lipopolysaccharide-stimulated raw 264.7 macrophage inducible nitric oxide synthase and nitric oxide production is decreased by an omega-3 fatty acid lipid emulsion," *J. Surg. Res.*, 2008.
- [47] H. Prakash, S. Sekhar, K. Sampath-Kumara, and S. Niranjana, "Attenuation of reactive oxygen/nitrogen species with suppression of inducible nitric oxide synthase expression in RAW 264.7 macrophages by bark extract of *Buchanania lanzan*," *Pharmacogn. Mag.*, vol. 11, no. 42, p. 283, Mar. 2015.
- [48] J. J. Burmeister, K. Moxon, and G. A. Gerhardt, "Ceramic-Based Multisite Microelectrodes for Electrochemical Recordings," *Anal. Chem.*, vol. 72, pp. 187–192, 2000.
- [49] "8-TRK FM - Box of 3 - CenMeT Service Center." [Online]. Available: <http://www.ukycenmet.com/8-trk-fm-box-of-3/>. [Accessed: 12-Nov-2019].

- [50] B. A. Wagner, J. R. Witmer, T. J. van't Erve, and G. R. Buettner, "An assay for the rate of removal of extracellular hydrogen peroxide by cells," *Redox Biol.*, vol. 1, no. 1, pp. 210–217, 2013.
- [51] J. C. Zhuang and G. N. Wogan, "Growth and viability of macrophages continuously stimulated to produce nitric oxide," *Biochemistry*, vol. 94, pp. 11875–11880, 1997.
- [52] R. Korhonen, A. Lahti, M. Hämäläinen, H. Kankaanranta, and E. Moilanen, "Dexamethasone inhibits inducible nitric-oxide synthase expression and nitric oxide production by destabilizing mRNA in lipopolysaccharide-treated macrophages.," *Mol. Pharmacol.*, vol. 62, no. 3, pp. 698–704, 2002.
- [53] B. K. Huang and H. D. Sikes, "Quantifying intracellular hydrogen peroxide perturbations in terms of concentration," *Redox Biol.*, vol. 2, pp. 955–962, 2014.
- [54] B. Halliwell, "Cell culture, oxidative stress, and antioxidants: Avoiding pitfalls," *Biomed. J.*, vol. 37, no. 3, pp. 99–105, 2014.
- [55] J.-S. Hwang *et al.*, "Lipopolysaccharide (LPS)-stimulated iNOS Induction Is Increased by Glucosamine under Normal Glucose Conditions but Is Inhibited by Glucosamine under High Glucose Conditions in Macrophage Cells," *J. Biol. Chem.*, vol. 292, no. 5, pp. 1724–1736, 2017.
- [56] N. O. Al-Harbi *et al.*, "Dexamethasone Attenuates LPS-induced Acute Lung Injury through Inhibition of NF- κ B, COX-2, and Pro-inflammatory Mediators," *Immunol. Invest.*, vol. 45, no. 4, pp. 349–369, 2016.